FLUORESCENT NANOHYBRIDS BASED ON ASYMMETRICAL CYANINE DYES DECORATED CARBON NANOTUBES

by

ÖZGE ÇAVUŞLAR

Submitted to the Graduate School of Engineering and Natural Sciences
in partial fulfillment of
the requirements for the degree of
Master of Science

Sabancı University
Spring 2015

FLUORESCENT NANOHYBRIDS BASED ON ASYMMETRICAL CYANINE DYES DECORATED CARBON NANOTUBES

APROVED BY:

Asst. Prof. Fevzi Ç. Cebeci ……..
(Dissertation Supervisor)

Asst. Prof. Belkıs Atasever Arslan ……

Assoc. Prof. Kürşat Şendur ……

Dr. Hayriye Ünal ……
(Dissertation Co-Advisor)

Asst. Prof. Serkan Ünal ……

DATE OF APROVAL: ……

ABSTRACT

FLUORESCENT NANOHYBRIDS BASED ON ASYMMETRICAL CYANINE DYES DECORATED CARBON NANOTUBES

ÖZGE ÇAVUŞLAR

Master of Science Thesis, July 2015

ASST. PROF. FEVZİ ÇAKMAK CEBECİ

Keywords: Carbon Nanotubes, Asymmetrical Cyanine Dyes, Fluorescence

In this thesis, we focused on imparting new optical properties to carbon nanotubes (CNTs) to allow their optical detection and visualization in biomedical applications.

We investigated the interactions of CNTs and DNA wrapped CNTs with asymmetrical cyanine dye molecules to study the applicability of resulting hybrid materials to fluorescent based systems. When CNTs interacted with asymmetrical cyanine dyes, they constructed a light absorbing nanoarray. However, the fluorescence emission of the two component structure was quenched. Alternatively, when single stranded DNA (ssDNA) wrapped CNTs interacted with asymmetrical cyanine dye molecules not only the absorbance intensity was altered but also the fluorescence intensity increased several fold. The assembly of CNT/dye nanohybrids and ssDNA/CNT/dye nanohybrid was also demonstrated by a shift in Raman spectrum indicating noncovalent binding. The thermal stability of ssDNA/CNT/dye nanostructures was investigated by fluorescence-based thermal analysis. Additionally, individually dispersed ssDNA/CNT nanohybrids and ssDNA/CNT/dye nanohybrids were visualized by transmitted electron microscopy (TEM) and scanning electron microscopy (SEM). Moreover the fluorescence of three component nanohybrids was visualized with confocal microscopy. When CNTs were excited with UV light, they became fluorescent. We have demonstrated that ssDNA wrapped CNTs can act as a scaffold on which asymmetrical cyanine dyes can self-assemble with increased quantum yields. Our work demonstrates the first example that a fluorophore lights up when it binds CNTs, thus provides a novel approach for the fluorescent labeling of CNTs.

ÖZET

Bu tezde, karbon nanotüplerin (CNT) biyomedikal uygulamalarda optik olarak tespit edilebilmesi ve görüntülenebilmesi için CNT'lere yeni optik özellikler kazandırılması üzerine çalışılmıştır.

CNT'lerin ve DNA ile sarılı CNT'lerin, asimetrik siyanin boyaları ile etkileşimiyle oluşan hibrid yapıların floresan sistemlere uygulanabilirliği araştırılmıştır. CNT'lerin asimetrik siyanin boyaları ile etkileşmeleri sonucunda nonkovalent olarak birbirlerine bağlandıkları ve absorbanslarının arttığı gözlemlenmiştir. Böylece, CNT ve boya moleküllerinin ışık absorbe eden bir nano dizi oluşturdukları tespit edilmiştir. Ancak, elde edilen bu iki bileşenli yapının floresan özellik göstermediği görülmüştür. Buna alternatif olarak, DNA ile sarılı CNT'lerin asimetrik siyanin boyaları ile etkileşimleri incelendiğinde, absorbans spektrumunda oluşan değişikliklerin yanında CNT'lerin floresan hale geldiği de görülmüştür. Raman spektrumunda oluşan kaymalar ile kurulan CNT/boya nanoyapıları ve DNA/CNT/boya nanoyapıları arasındaki nonkovalent bağlanma kanıtlanmıştır. Floresan esaslı termal analiz ile DNA/CNT/boya nanoyapılarının termal stabilitesi araştırılmıştır. Ayrıca, geçirmeli elektron mikroskobu (TEM) ve taramalı elektron mikroskobu (SEM) ile DNA/CNT nanoyapılarının disperse oldukları gözlemlenmiştir. Bunlara ek olarak, üç bileşenli yapılar konfokal mikroskopi ile görüntülenmişlerdir. CNT'ler UV ışığı ile uyarıldıklarında floresan hale gelmişlerdir. Çalışmalarımız sonucunda, DNA ile sarılı CNT'lerin asimetrik siyanin boyalarının bağlanması ve floresan hale gelmeleri için uygun bir iskelet görevi gördüğü gösterilmiş, ilk defa boya moleküllerinin CNT'lere bağlandığında floresan hale geldiği bir yapı ortaya konulmuş, böylece CNT'lerin floresan etiketlenmeleri konusunda yeni bir yaklaşım sunulmuştur.

Dedicated to my family,

ACKNOWLEDGMENTS

First of all, I would like to thank my advisor Asst. Prof Fevzi Çakmak Cebeci, and my co-advisor Dr. Hayriye Ünal for their patience and direction during my master degree.

I sincerely thank my best friends from Sabancı University Aysu Yurduşen and Yonca Yakut, from ITU, Anıl Ayşe Yeşildağ, Merve Akarlı and Nevin Yılmaz for their cheerful friendship, endless support and understanding. Also I would like to thank Cenk Yanık for his support to write this thesis.

I wish to express my appreciation to Dr. Serap Hayat Soytaş for her help with TEM analysis and Dr. Meltem Sezen for her help with SEM analysis.

Finally I would like to thank my family who believed in me from the beginning: my mother Fatma GÜRAN, my father Mehmet GÜRAN, my sisters Gizem ÇAVUŞLAR-ERDOĞAN and Megan GISCLON and my brother-in-law Halit ERDOĞAN, my grandparents and my uncle Doç. Dr. Salih GÜRAN. I deeply appreciate their huge efforts. Without their support, patience and love I could not have achieved all of this.

This thesis was funded by TUBITAK (Grant No: 113M144).

July 2015 Özge ÇAVUŞLAR

TABLE OF CONTENTS

LIST OF FIGURES

LIST OF TABLES

ABBREVIATIONS

CNT:	Carbon Nanotubes
ssDNA:	Single stranded DNA
dsDNA:	Double stranded DNA
YO:	Oxazole yellow
TO:	Thiazole orange

CHAPTER 1 GENERAL INTRODUCTION

1 Carbon Nanotubes

Ever since the discovery of carbon nanotubes (CNTs) in 1991 by Iijima, chemists, biologists, physicists and scientists from other fields have been fascinated by their unique properties such as electronic, thermal, mechanical, magnetic and superconducting properties [1-7]. CNTs are allotropes of carbon with a nanostructure. The difference of CNTs from other allotropes of carbon such as graphite, diamond and fullerene (C60, C70, etc.) is that CNTs can possess aspect ratio larger than 1000 [5]. Bonding in nanotubes is typically sp^2 [8] [9]. CNTs can be divided into two main groups such as single-walled carbon nanotubes (SWCNTs) and multi-walled carbon nanotubes (MWCNTs) [7] (Figure 1).

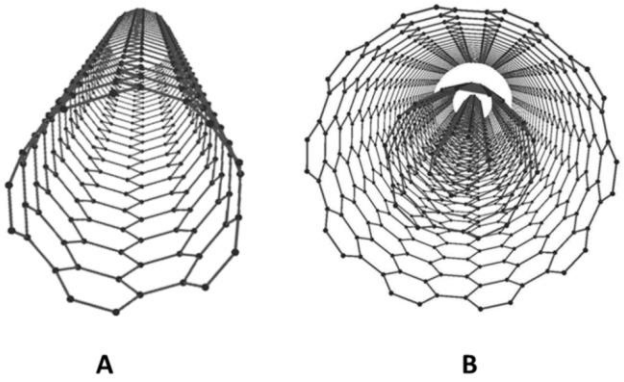

Figure 1 Schematic representation of (A) single-walled carbon nanotubes (SWCNT) and (B) multi-walled carbon nanotubes (MWCNT) [10].

The sp^2 bond structure of CNTs provides stiffness and strength [11]. In addition to sp^2 bond structure, π-σ hybridization allows altered chemical reactions [12]. Although mechanical, chemical and electronic properties of CNTs have wide application areas, the utilization of optical properties of CNTs have been improving.

1.1 Functionalization of Carbon Nanotubes

Due to hydrophobicity of pristine CNTs, it is difficult to disperse them [13]. CNTs need processing such as purification and functionalization after their synthesis for further applications. After the synthesis of CNTs, metal nanoparticles and amorphous carbon exist as a residue [14]. For removing the residue, CNTs need to be decontaminated by purification methods such as chemical, physical and a combination of both [15].

The method of the chemical purification is built on the dissolution of metallic impurities by acids and a selective oxidation, where CNTs are oxidized at a slower rate than carbonaceous impurities. The physical purification method isolates CNTs from impurities based on the differences in their physical size, aspect ratio, gravity, and magnetic properties, etc. The third method is the combination of chemical and physical methods which can lead to high yield and quality CNT products [15].

CNT walls are chemically stable due to the aromatic nature of the bonds between carbon atoms [5]. Thus, the surface of CNTs needs to be functionalized for being utilized in different applications. The chemistry of functionalization of CNTs and the reaction mechanisms between the CNTs and functional groups have been described in several inclusive review papers [16-19]. Functionalization of CNTs can be categorized as covalent functionalization and noncovalent functionalization due to the interactions between the active molecules and carbon atoms on the CNTs [5].

1.1.1 Covalent Functionalization of Carbon Nanotubes

Covalent functionalization occurs via the covalent linkage of functional groups onto carbon scaffold of CNTs. The aromatic nature of the sidewall can be modified by the direct covalent sidewall functionalization via the change of hybridization from sp^2 to sp^3 and the resulting loss of π conjugation system on graphene layer (Figure 2). The direct covalent sidewall functionalization occurs with the reaction between CNTs and highly reactive chemicals such as fluorine and chlorine. Moreover, cycloaddition reactions such as Diels-Alder reaction, carbene and nitrene addition, chlorination, bromination, hydrogenation, azomethine ylides, have also been effectively utilized. Defect functionalization is an additional technique for covalent functionalization [5]. Defects can be formed by an oxidative process with strong

acids such as HNO_3, H_2SO_4 or a mixture of them, or with strong oxidants such as KMnO4, ozone, reactive plasma [5].

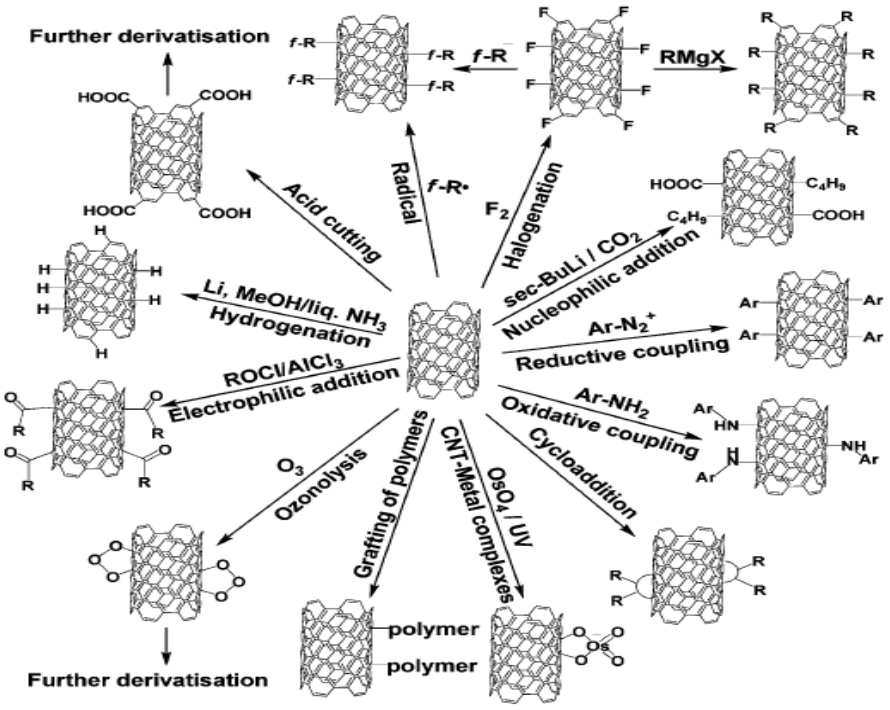

Figure 2 Surface functionalization of carbon nanotubes [20].

1.1.2 Noncovalent Functionalization of Carbon Nanotubes

Since the π electron system is responsible for the electrical and thermal transport in CNTs structure, the covalent functionalization may lead to the disruption of π electron system in nanotubes.

On the other hand, noncovalent functionalization is an alternate process for modification of the interfacial characteristics of nanotubes [5]. Noncovalent functionalization is based on van der Waals forces, hydrogen bonds, electrostatic forces and π stacking interactions [21]. There are three different methods to functionalize CNTs noncovalently. Figure 3-A is representing one of the methods which is polymer wrapping. CNTs disperse in the presence of polymers. The interactions between CNTs and polymers are the van der Waals interactions and π-π stacking due to aromatic rings in the structures of CNTs and polymers. Another method to noncovalently functionalize CNTs is utilizing surfactants (Figure 3-B). The mechanism is that surfactants lower the surface tension of CNTs due to the physical adsorption on the CNTs

surface. Thus, the creation of aggregates is prohibited efficiently. Endohedral method showing in Figure 3-C is an alternative technique for the functionalization. In this method, guest atoms or molecules are deposited inside the holes of CNTs as a result of capillary effect.[5]

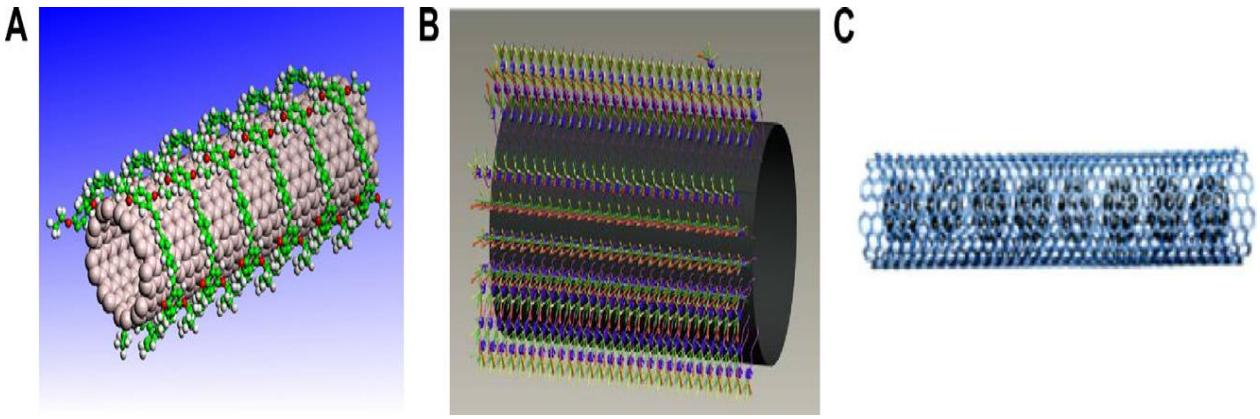

Figure 3 Pictures of different methods of noncovalent functionalization of CNTs (A: polymer wrapping; B: surfactant adsorption; C: endohedral method) [5].

Deoxyribonucleic acid (DNA) is a naturally occurring polymer. Most of DNA molecules are made of two polymer strands bound noncovalently which is called double stranded DNA (dsDNA). When dsDNA is exposed to heating processes, these strands become apart from each other and form two single stranded DNA (ssDNA). These strands are composed of nucleobases such as guanine, cytosine, adenine and thymine. As it is seen in Figure 4, nucleobases are aromatic molecules that have double bonds on their structures.

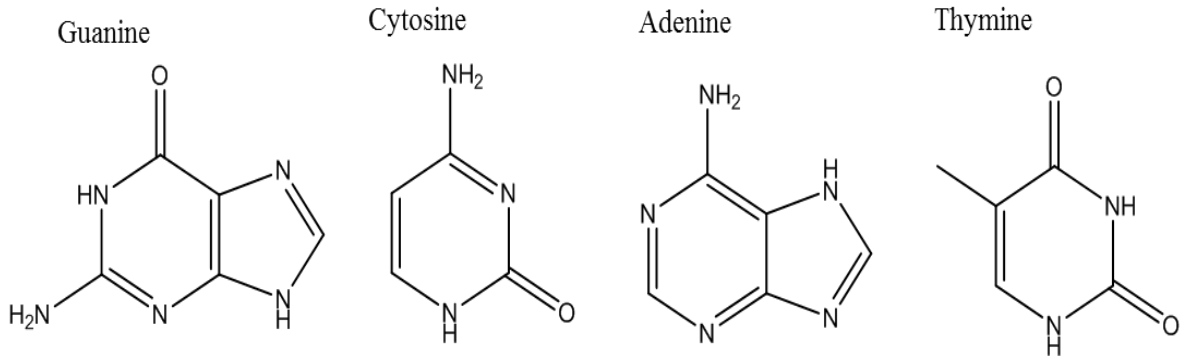

Figure 4 Structures of DNA nucleobases.

Zheng and his team were inspired from the π stacking interactions between nucleobases. Thus they demonstrated short ssDNA (30-90 bases) can bind to SWCNT under ultrasonication noncovalently (Figure 5) [22]. Moreover their study proved that not only sequence and length of DNA affect the dispersion but also diameter and chirality of CNT is essential for dispersion [23]. Their research studies 'open the door to carbon nanotube based applications in biotechnology'[22].

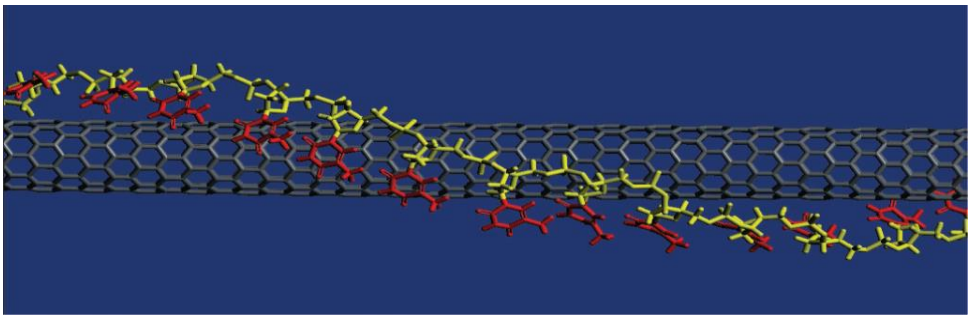

Figure 5 Binding model of ssDNA and SWCNT [22].

1.2 Fluorescent Labeling of Carbon Nanotubes

Recent research studies of CNTs are focused on their interactions with fluorophores mainly to investigate the tunable optical properties of resulting hybrids and their applications. One of the main goals of studying the interactions of CNTs with fluorophores is utilization of CNTs for photoactive applications such as photovoltaic cells, donor-acceptor probes and photothermal agents [24, 25]. Another goal for studying these interactions is the fluorescent labeling of CNTs for biomedical applications. CNTs are widely utilized for biomedical applications such as in vivo imagining, drug & gene delivery, utilization as growth substrates and biomimetic implants [26]. He and coworkers summarized these applications as demonstrated in Figure 6.

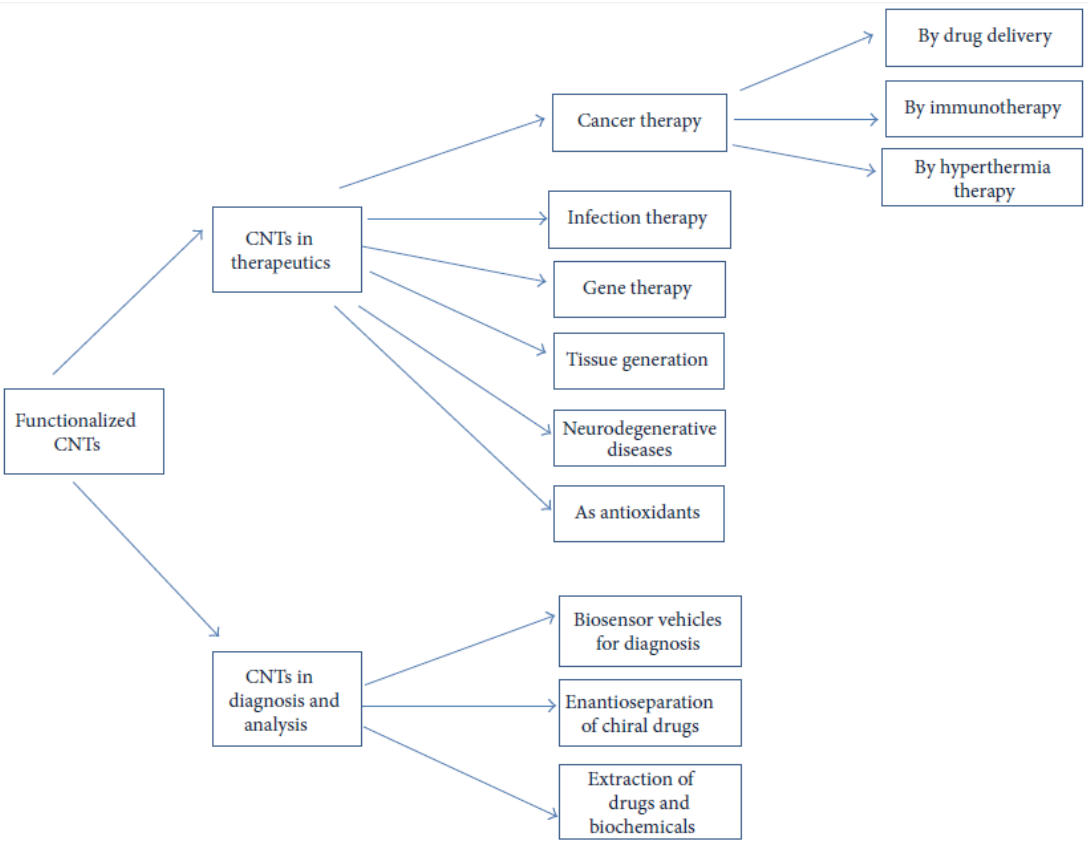

Figure 6 Schematic of carbon nanotube applications in therapeutics and biomedical diagnosis and analysis [27].

Visualization of CNTs is critical for the biomedical applications of CNTs. The conventional method for the visualization of CNTs, that is electron microscopy, is not feasible in biological environments. Classical optical microscopy, is not practical considering the nanosizes of CNTs. Fluorescence microscopy on the other hand offers higher resolution, but it requires that the objects to be visualized are tagged with a fluorophore. Therefore, fluorescent labeling of CNTs is a promising topic for researchers.

Fluorescein is one of the common fluorophores utilized for the labeling of biomolecules. Due to π-stacking, they interact with CNTs intensely. Nakayama-Ratchford and his team decorated CNTs with fluorescein-polyethylene glycol under ultrasonication [28]. Also Yoshimura and his team used commercial fluorescein molecules such as Texas red hydrazine and BODIPY FL hydrazine to label CNTs [29] Fluorescein molecules have pH-dependent optical absorbance and fluorescence [30].

Prakash and his team reported fluorescent labeling of MWCNTs with several fluorophores such as symmetrical carbocyanines and fluorescein in polar and nonpolar solutions [31].

Anthracene is another fluorescent molecule which was used by Zhang and his team. They utilized different derivatives of the anthracene such as anthracene, anthraobin, 9,10-dibromoantharacene, 9,10-anthracenedicarbonitrile and 9-anthracenemethanol with the intention of determine the effect of different substituents on electronic properties of SWCNT [32].

Martin and his team reported the change in photopysical properties of functionalization of MWCNT and SWCNT by using dendra and tethered pyrene species [33].

Satake's team used tetraformylpophryins for labeling CNTs. Moieties of porphyrins was almost quenched inside the composite [34]. Moreover, the interactions between SWCNT and porphyrins to electron donor-acceptor nanohybrids structures were investigated [35, 36].

Pan et al. examined the interactions between CdSe quantum dots (QD) and MWCNTs to investigate the optical properties of CNT/QD hybrid materials [37].

Furthermore, fluorescent polymers were studied for fluorescent labeling CNTs [38-40].

While these studies proved noncovalent binding interactions between fluorescent molecules and CNTs, all of them resulted in quenching of the fluorescence upon binding to CNTs leading to weak fluorescence. A method that allows fluorescence enhancement of fluorophores upon binding to CNTs has not been reported.

Asymmetrical cyanine dyes are also fluorescent molecules which are widely used as light-up probes due to the interactions with dsDNA. Moreover, the interactions between asymmetrical cyanine dyes and CNTs have not been researched yet. Thus in this thesis, noncovalent interactions of asymmetrical cyanine dyes and CNTs were investigated.

2 Cyanine Dyes

Cyanine dyes are broadly utilized owing to their advantageous fluorescence properties. Cyanine dyes have wide biological applications. They have been used as donors/acceptors in fluorescence resonance energy transfer (FRET) based methods, and as covalent labels for nucleic acid sequencing, fluorescence *in situ* hybridization (FISH), and for the imaging of single molecules in living cells [41]. General structure of cyanine dyes consist of two nitrogen

atoms, one of them is positively charged, linked by a conjugated chain of several numbers of carbon atoms which is often polymethine chain. The positive charge is delocalized through the methine chain to other nitrogen [42]. The conjugation causes extremely colored crystals and solutions.

Cyanine dyes can be classified into two; symmetrical and asymmetrical cyanine dyes due to the symmetry of the chromophore groups (Figure 7). Symmetrical cyanine dyes consist of same heterocycles linked at the same position. Asymmetrical cyanine dyes are made of two different heterocycles or two identical heterocycles linked at the different positions. The types of dyes presented in this thesis are asymmetrical cyanine dyes.

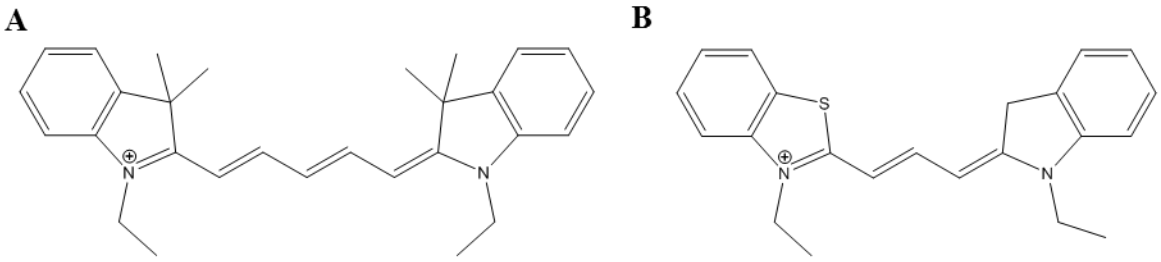

Figure 7 The examples of (A) symmetrical and (B) asymmetrical cyanine dyes [42].

Asymmetrical cyanine dyes have unique photophysical properties. Due to the twisting around the methine bridge that connects the aromatic rings, their fluorescence is quenched when they are free in solution. But when they are in a restrictive environment such as between the base pairs of double stranded DNA (Figure 8), their fluorescence intensity increases several fold [43]. The fluorescence quantum yield of Thiazole orange (TO) rise 18900 times upon binding to DNA has been testified [44]. The binding mode is intercalative according to linear dichroism and NMR measurements [45].

For this thesis we used thiazole orange (TO), the cationic derivative of thiazole orange (TO-PRO-1), TO-PRO-3 which is analogous to TO-PRO-1 but has a longer methine bridge, the cationic derivative of oxazole yellow (YO-PRO-1) and its dimeric form (YOYO-1)

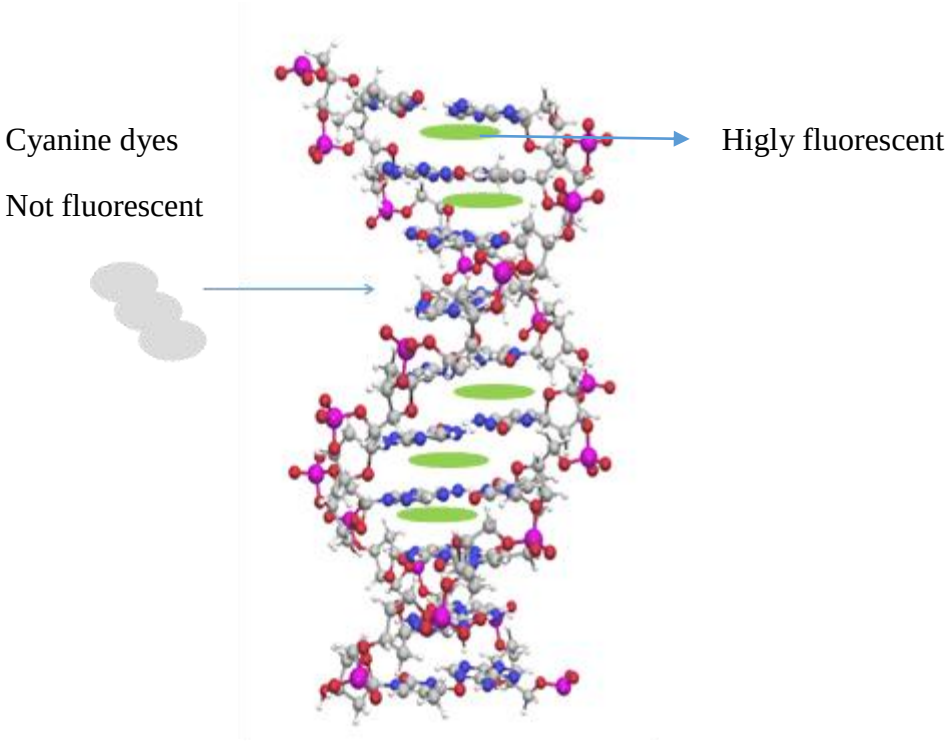

Figure 8 Schematics of intercalation of cyanine dyes into DNA.

This thesis was also published as ‘Self-assembly of DNA wrapped carbon nanotubes and asymmetrical cyanine dyes into fluorescent nanohybrids’ (RSC Adv., 2015, 5, 22380).

CHAPTER 2 INVESTIGATION OF INTERACTIONS BETWEEN CARBON NANOTUBES AND ASYMMETRICAL CYANINE DYES

1 Introduction

To detect and visualize CNTs with fluorescence microscopy, decorating CNTs with fluorophores is required. In previous studies, interactions between CNTs and several fluorophores such as fluorescein, symmetrical carbocyanines, anthracene, pyrene, porphyrin, quantum dots and fluorescent polymers were investigated. The main problem of labeling CNTs with fluorescent molecules is that noncovalent interactions lead to a decrease in the fluorescence emission due to electron and energy transfer [46, 47]. To improve fluorescent labeling of CNTs, new methods need to be developed where the fluorescence emission does not decrease when the fluorophore binds to CNT.

As it was mentioned in Chapter 1, CNTs are hollow cylindrical tubes that are made of one or more centered sheets of sp^2 hybridized carbons [48]. Similarly, asymmetrical cyanine dyes also have sp^2 hybridized carbons on their structure. Based on this similarity on the electronic structure, we hypothesized that asymmetrical cyanine dyes can have non-covalent interactions with CNTs due to π-π stacking and can result in CNT/dye hybrid structures that are fluorescent (Figure 9).

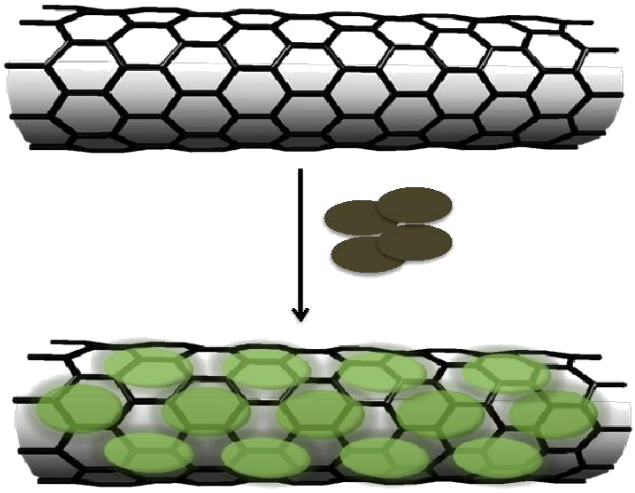

Figure 9 Schematic representation of fluorescent labeling of CNTs

For this thesis we used thiazole orange (TO), the cationic derivative of thiazole orange (TO-PRO-1), TO-PRO-3 which is analogous to TO-PRO-1 but has a longer methine bridge, the cationic derivative of oxazole yellow (YO-PRO-1) and its dimeric form (YOYO-1) (Figure 10). This set of asymmetrical cyanine dyes allowed us to study the effect of charge and size of the dye molecule on the interactions with CNTs.

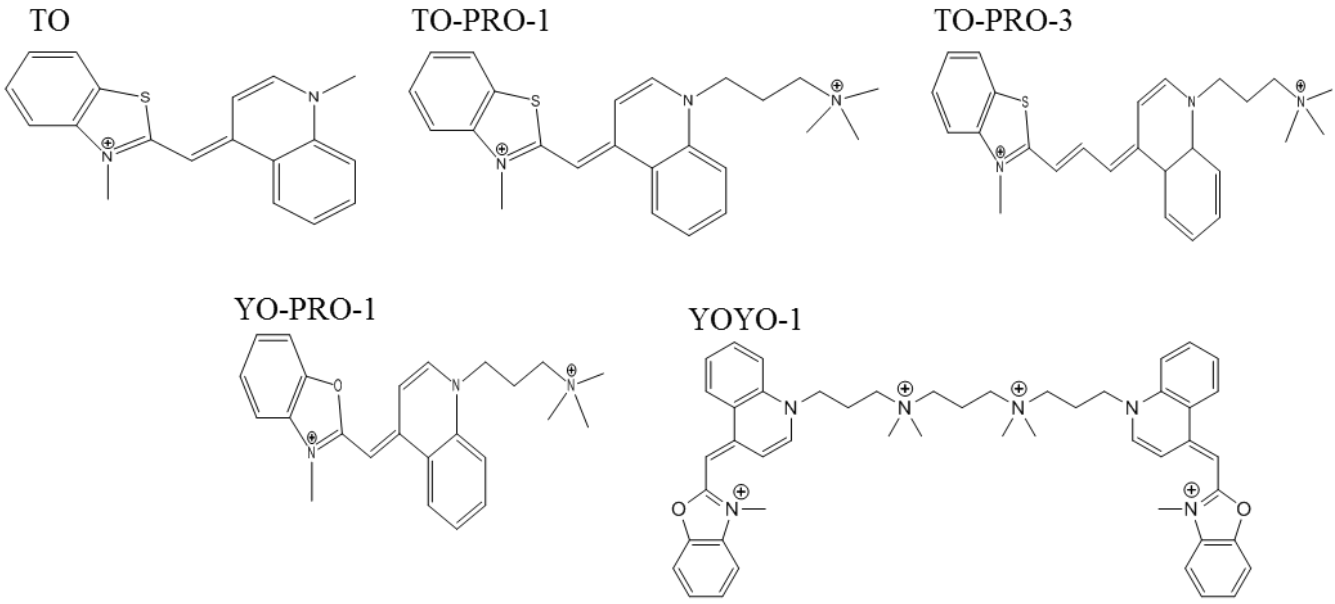

Figure 10 Structures of asymmetrical cyanine dyes

2 Materials and Methods

2.1. Materials

Asymmetrical cyanine dyes (Figure 10) YO-PRO-1 (Y3603), TO-PRO-1 (T3602), YOYO-1 (Y3601), and TO-PRO-3 (T3605) were purchased from Life Technologies. TO was purchased from Sigma Aldrich. CNTs were purchased from Cheap Tubes Inc. in the form of dry powder. The purity of CNTs as declared by the supplier is >99% for SWCNTs, >99% for MWCNTs and >60% for DWCNTs. The outer diameter of CNTs as stated by the supplier is 1-2 nm for SWCNTs, 2-4 nm for DWCNTs and <20 nm for MWCNTs. The length of CNTs as specified by the supplier is 3-30 nm for SWCNTs, ~50 nm for DWCNTs and 1-12 μm for MWCNTs. Centrifugal filter devices with a 30 kDa cut-off membrane (Microcon-30 kDa) were purchased from Millipore. 1X PBS buffer was prepared by mixing 137mM NaCl, 2.7 mM KCl, 10 mM Na_2KPO_4 and 1.8 mM KH_2PO_4 pH=7.4.

2.2 Methods

2.2.1 Experimental

As the general protocol, calculated amounts of dyes and CNTs were sonicated in an ice bucket to obtain asymmetrical cyanine dyes/CNT nanohybrids followed by ultracentrifugation at high speed to remove undispersed CNTs. Next, unbound dye molecules are removed. In order to optimize the parameters, 35 different samples were prepared. Optimum parameters for preparation of CNT/asymmetrical cyanine dye nanohybrids are as follows: 0.5 mL of dispersal solution containing 0.1 mg/mL CNTs and 30 μM asymmetrical cyanine dyes was prepared. The solution was sonicated with a microprobe (Q Sonica, Q700) for 30 min, with 2 seconds pulse on and 5 seconds pulse of in ice. The dispersion was ultracentrifuged at 14 000 rpm for 10 min and the supernatant that is the black colored dispersion was removed into a clean eppendorf tube labeled as CNT/dye dispersion. In order to remove the unbound dye molecules, the dispersion was transferred into a Microcon centrifugal filter device and centrifuged at 14 000 rpm until the filtrate volume is reduced to approximately 50 mL. The filtrate that remains in the filter device was recovered and diluted to 500 mL with water.

2.2.2 Characterizations

For Raman Spectroscopy analysis 10 µL drops of 30 µM of dye and 0.1 mg/mL of CNT dispersions were dried on silicon wafers and measurements were made on a Renishaw in Via Reflex Raman Spectrometer set with a 532 nm laser. Absorbance measurements were made on a Cary 5000 Spectrophotometer. 30 µl of dye and 0.1 mg/mL of CNT dispersions were transferred into 500 µl quartz cuvettes and scanned 200-800 nm. Fluorescence analysis was made on a Cary Eclipse Fluorescence Spectrophotometer. Measurements were made in 500 µl quartz cuvettes. Dyes and Dye/SWCNT conjugates were excited at the following wavelengths: TO: 490nm, TO-PRO-1: 490nm, TO-PRO-3: 620nm, YO-PRO-1: 480nm, YOYO-1: 480nm. The bandwidth for excitation and emission was 5nm.

3 Results and Discussion

3.1. Dispersion Studies

In order to investigate interactions between asymmetrical cyanine dyes and CNTs, CNTs were ultrasonicated in aqueous dye solutions. Firstly, to determine whether SWCNTs can interact with asymmetrical dyes, 500 µM TO in 1X PBS buffer was mixed with 0.6 mg/mL of SWCNT. The solution was sonicated with a microprobe for 2 min, at 50% amplitude. As demonstrated in Figure 11, SWCNTs were not dispersed in TO solution; instead they were aggregated into bundles forming a black precipitate. The fact that the supernatant does not have the orange color of the TO solution indicates binding of the dye molecules to SWCNTs which cannot be dispersed.

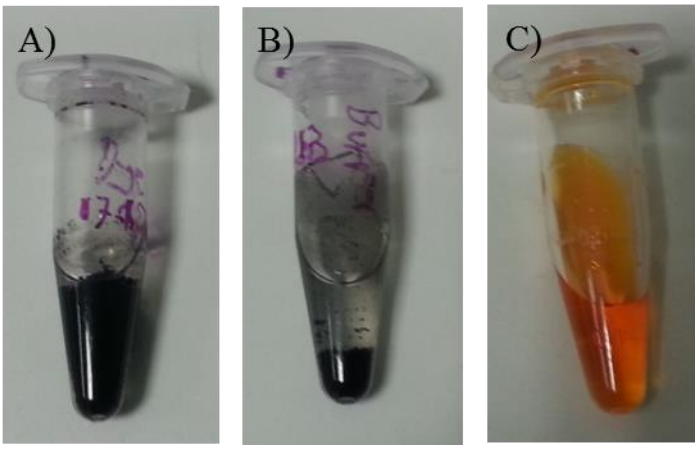

Figure 11 Pictures of the Sample-1 (A) SWCNTs ultrasonicated in PBS buffer containing TO. (B) SWCNTs ultrasonicated in PBS buffer. (C) TO ultrasonicated in PBS buffer.

To understand reasons of failure to dispersion and change in color of dye, parameters of the dispersion solution were changed, which is given in Table 1. The parameters we focused on were as follows:

1) *Duration of sonication*: The duration of sonication was adjusted in order to see the effect of total energy applied to the sample on the quality of the dispersion. As an additional parameter the pulse on/off time was also adjusted in order to determine the optimal conditions that prevent the overheating of the sample.
2) *CNT concentration:* The concentration of CNT in the dispersion solution was adjusted. In higher concentrations of CNTs, they can interact with each other due to van der Waals forces and aggregate [5]. Thus, with the aim of decreasing the intermolecular interactions within CNTs, concentration of CNTs was decreased from 0.6 mg/mL to 0.1 mg/mL.
3) *Ionic concentration of the dispersion solution:* Researchers from biochemical and colloidal sciences reported that the stability of biomolecules and colloidal dispersions can be affected by ions, and ions can interact with them in different ways. The study by Frovol and his team proved that in the presence of salt CNT concentration in the dispersion decreased due to interactions between ions and the CNT surface [49]. In order to investigate whether SWCNT/TO dispersion can be obtained in the absence of salt, PBS buffer was exchanged with deionized H_2O. As an alternative, DMSO,

and a surfactant containing solution (Triton X-100) were also used as the medium of the dispersion.

4) *Dye concentration:* Asymmetrical cyanine dyes are known to form J-type, and H-type aggregates due to intermolecular noncovalent interactions including π-π stacking and hydrophobic forces. Thus, in order to form SWCNT/dye hybrid structures the dye concentration should be adjusted to an optimum value at which dye molecules prefer to bind the CNTs instead of other dye molecules. The concentration of dye molecules were adjusted to determine the optimum conditions that would favor the dispersion of CNTs by the formation of CNT/dye hybrid nanostructures.
5) *The type of CNTs:* MWCNTs were also used in addition to SWCNTs, to investigate the effect of CNT diameter on the CNT/dye dispersion.

Table 1 List of samples which have different parameters

Sample	CNT type	[CNT] (mg/mL)	Buffer	[TO] (μM)	Amplitude (%)	Duration of sonication (min)
1	SWNT	0.6	PBS	500	50	2
2	SWNT	0.6	PBS	500	50	15
3	SWNT	0.6	PBS	500	50	30
4	SWNT	0.6	DMSO	500	50	30
5	SWNT	0.1	PBS	500	50	30
6	SWNT	0.1	PBS	500	50	30
7	MWNT	0.02	PBS	500	70	30
8	MWNT	0.1	PBS	500	70	30
9	MWNT	0.1	H_2O	500	70	30
10	MWNT	0.01	H_2O	500	70	30
11	MWNT	0.1	H_2O	500	70	30
12	MWNT	0.1	Triton-X100	500	70	20
13	MWNT	0.1	H_2O	100	70	30

Among all the samples demonstrated in Table 1, Sample 13 resulted in a stable dispersion indicating optimal conditions for the preparation of CNT/TO nanohybrids. For the preparation of this sample, 100 μM aqueous solution of TO dye was ultrasonicated with 0.1 mg/ml of MWCNTs. Following the ultrasonication the dispersion was centrifuged at high speed to remove undispersed MWCNTs. Figure 12-A shows the resulting dispersion of

MWCNTs in aqueous TO solution. As seen on the picture a brown-colored stable dispersion was obtained. As a control, the same amount of MWCNTs was ultrasonicated in water by applying the same sonication conditions. As seen in Figure 12-B MWCNTs alone were not dispersed in water, indicating MWCNTs were dispersed only due to the noncovalent interactions formed between MWCNTs and TO molecules. The fact that a dispersion was obtained demonstrates that CNTs can exhibit noncovalent interactions with the asymmetrical cyanine dye and result in CNT/dye hybrid nanostructures.

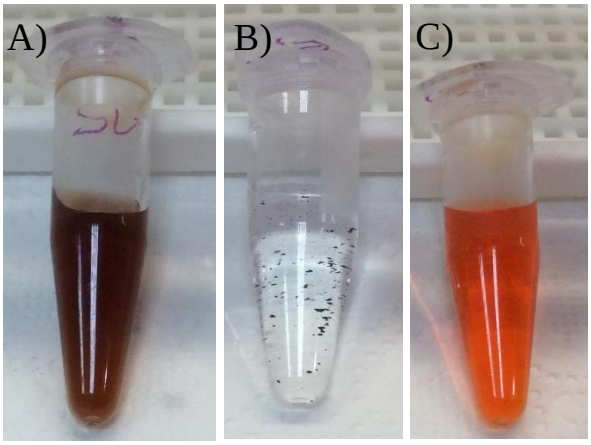

Figure 12 Pictures of the Sample-1 (A) MWCNTs ultrasonicated in aqueous solution of TO (B) MWCNTs ultrasonicated in water (C) TO ultrasonicated in water.

After initial optimization studies for the preparation of CNT/asymmetrical cyanine dye nanohybrids, samples that contain different types of CNTs and varying types of asymmetrical cyanine dyes were prepared to further study the resulting nanohybrids.

The samples were prepared according to the following protocol. The dispersal solution containing 0.1mg/mL MWCNTs and 30 μM dye was sonicated with a microprobe for 30 min with 2 seconds pulse on and 5 seconds pulse off time in ice. The dispersion was ultracentrifuged at 14 000 rpm for 10 min and the supernatant that is the black colored dispersion was removed into a clean eppendorf tube labeled as CNT/dye dispersion. In order to remove the unbound dye molecules, the dispersion was transferred into a Microcon centrifugal filter device and centrifuged at 14 000 rpm until the filtrate volume is reduced to approximately 50 mL. The filtrate that remains in the filter device was recovered and diluted to 500 mL with water.

CNT/Dye Nanohybrids with CNTs of Different Diameters:

To determine whether CNTs of different diameters can exhibit noncovalent interactions with the asymmetrical cyanine dyes, CNT/dye nanohybrids were prepared by using single walled (SWCNT), double walled (DWCNT), and multi walled (MWCNT) CNTs. 0.1 mg/ml of SWCNTs, DWCNTs, and MWCNTs were ultrasonicated in an aqueous TO solution, followed by ultracentrifugation to remove unbound CNTs. As can be seen in Figure 13, independent of their diameters, MWCNTs, DWCNTs, and SWCNTs were able to be dispersed in the presence of TO dye. This result further demonstrates that asymmetric cyanine dyes can form noncovalent interactions with the sidewalls of CNTs of different structures.

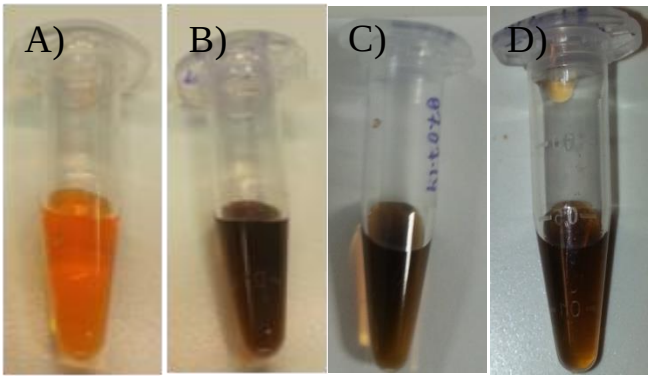

Figure 13 Pictures of (A) TO (B) MWCNTs ultrasonicated in aqueous solution of TO. (C) DWCNTs ultrasonicated in aqueous solution of TO. (D) SWCNTs ultrasonicated in aqueous solution of TO.

CNT/Dye Nanohybrids with asymmetrical cyanine dyes of different structures:

Furthermore, to investigate whether CNTs can be dispersed by asymmetrical cyanine dyes of different structural and spectral properties MWCNTs were ultrasonicated in aqueous solutions of TO-PRO-1, TO-PRO-3 YO-PRO-1 and YO-YO-1. As demonstrated in Figure 14, MWCNTs were finally dispersed in all of the dye solutions as can be seen by the darker colors of the resulting mixtures. Different sizes and charges depending on the chemical structure of each dye did not have significant effect on noncovalent binding interactions and each of the dye was able to turn bundles of MWCNTs into individually dispersed MWCNTs potentially through π- π stacking interactions.

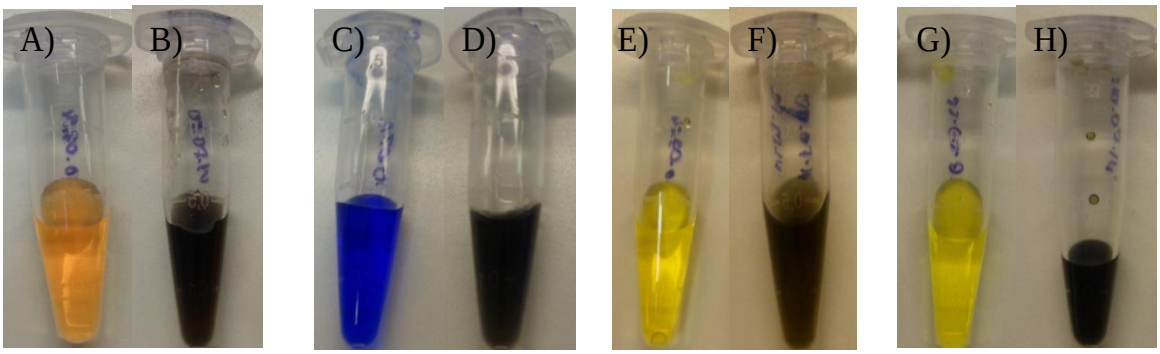

Figure 14 Pictures of (A) TO-PRO-1 (B) MWCNTs ultrasonicated in aqueous solution of TO-PRO-1. (C) TO-PRO-3 (D) MWCNTs ultrasonicated in aqueous solution of TO-PRO-3. (E) YO-PRO-1 (F) MWCNTs ultrasonicated in aqueous solution of YO-PRO-1. (G) YOYO-1 (H) MWCNTs ultrasonicated in aqueous solution of YOYO-1.

As a conclusion for the dispersion studies, CNT/asymmetrical cyanine dye nanohybrids were unstable in the presence of ions, as Frolov and co-workers specified in their study, ions and sidewalls of CNTs had an undesirable interactions and ruined the stability of CNT dispersion [49]. On the other hand CNTs formed stable dispersions in water. Moreover, higher concentrations of CNTs decrease the stability due to van der Waals forces, probably because of the formation of asymmetrical cyanine dye aggregates at higher concentrations. While CNTs were not dispersed in water, in the presence of asymmetrical cyanine dyes, CNTs constructed stable dispersions under same conditions. This result demonstrates that CNT and asymmetrical cyanine dyes can have strong non-covalent interaction possibly because of π-π stacking between aromatic moeities.

Additionally, CNT/dye dispersions were stable without any precipitation of CNTs for more than 1 month. In order to prove non-covalent interactions quantitatively, spectroscopic methods were used such as Raman spectroscopy and UV-Vis spectroscopy.

3.2. Raman Spectroscopy

Raman spectroscopy demonstrated the changes in the electronic structure of CNTs upon binding to asymmetrical cyanine dyes. The tangential stretch G-band is an intrinsic feature of a carbon nanotube closely related to vibrations in all sp^2 hybridized carbon materials. Figure 15-A demonstrates the spectrum of pristine MWCNT in comparison to TO/MWCNT dispersion. While the G band of pristine MWCNT is at 1570 cm^{-1}, this band exhibits an upshift to 1575 cm^{-1} when the MWCNT is bound to TO. This shift illustrates the change on

electronic structure of carbon nanotubes as a result of noncovalent interaction [50, 51]. A similar shift of G band was observed for TO/SWCNT, TO/DWCNT and TO-PRO-1/MWCNT, TO-PRO-3/MWCNT, YO-PRO-1/MWCNT and YOYO-1/MWCNT dispersions (Figure 14).

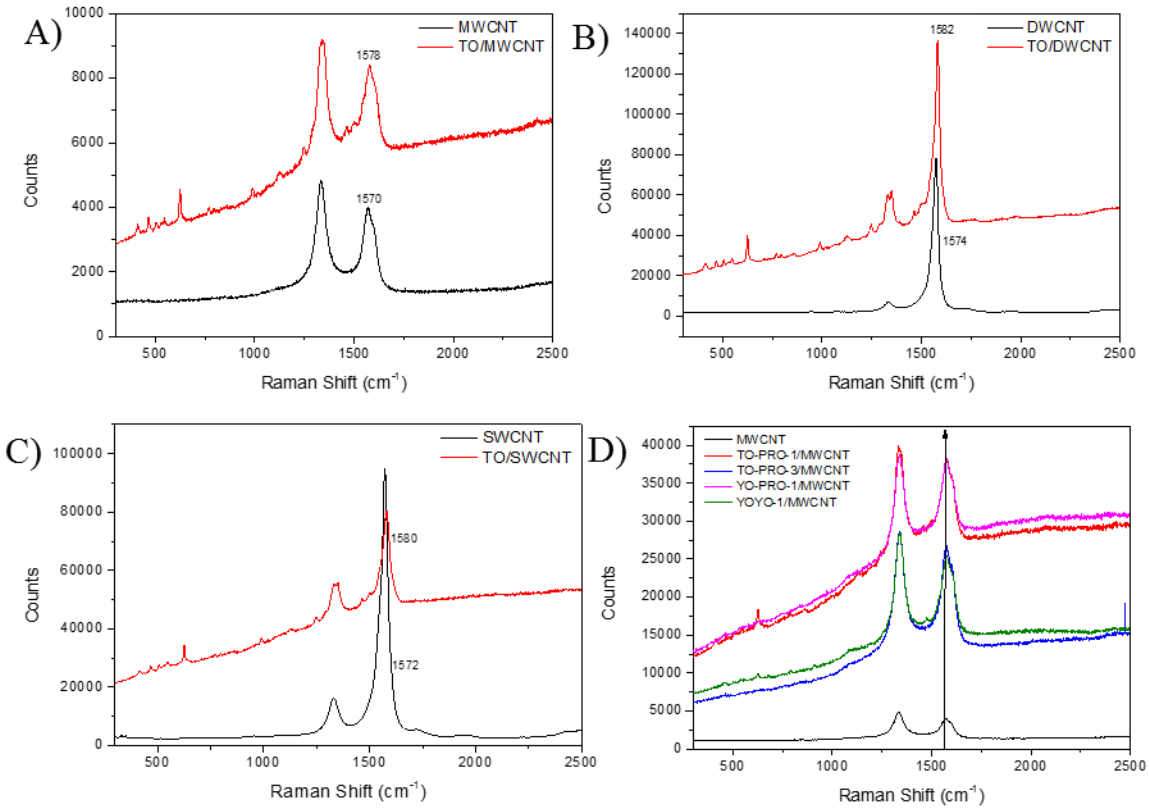

Figure 15 Raman spectra comparison of (A) MWCNT and TO/MWCNT dispersion. (B) DWCNT and TO/DWCNT dispersion. (C) SWCNT and TO/SWCNT dispersion. (D) MWCNT, TO-PRO-1/MWCNT, TO-PRO-3/MWCNT, YO-PRO-1/MWCNT and YOYO-1/MWCNT dispersions.

3.3 UV-Vis Spectroscopy

UV-vis spectroscopy further demonstrated the change in the electronic structure of dye molecules upon binding to CNTs. Figure 16 shows the absorbance spectra of comparison of TO vs. TO/MWCNT, TO/DWCNT and TO/SWCNT dispersions which are corrected for CNT absorbance in this wavelength range. While the unbound dye has the highest intensity, intensity of absorbance decreases when the dye is bound to MWCNTs, DWCNTs, and SWCNTs. According to the Lambert-Beer equation the change in absorbance intensity is

related to concentration of dye (c) and molar extinction coefficient (ε). Since the concentrations of dyes were equal, molar extinction coefficient of TO possibly was changed due to noncovalent interaction between CNTs and asymmetrical cyanine dye. Since the TO/SWCNT has the largest change in molar extinction coefficient of TO, the interactions between TO and SWCNT are presumed to be stronger.

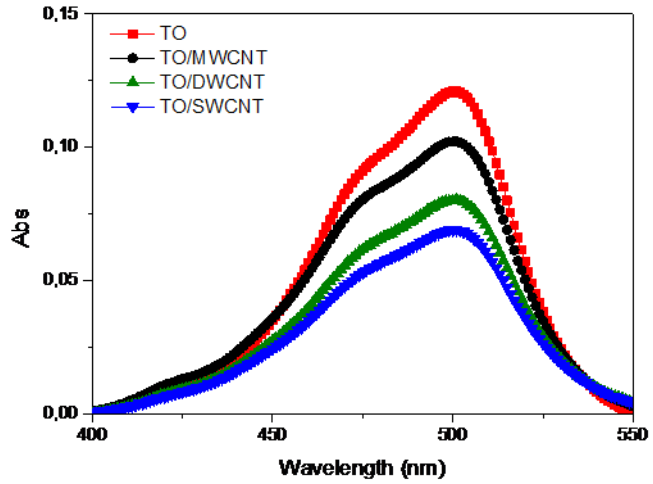

Figure 16 Absorbance spectra of 30µM TO, 30µM TO/MWCNT, 30µM TO/DWCNT and 30µM TO/SWCNT dispersions.

Figure 17 illustrates the UV-Vis absorbance spectra recorded for TO-PRO-1/MWCNT, TO-PRO-3/MWCNT, YO-PRO-1/MWCNT and YOYO-1/MWCNT dispersions which are corrected for MWCNT absorbance in this wavelength range and normalized between 0 and 1. In Figure 17-A, the black spectrum is unbound TO-PRO-1. The peak at 480 nm represents dimer molecules and the peak at 500 nm represents monomer molecules [43]. In Figure 17-B, the black spectrum is unbound TO-PRO-3. The peak at 590 nm represents dimer molecules and the peak at 630 nm represent monomer molecules. In Figure 17-C, the black spectrum is unbound YO-PRO-1. The peak at 460 nm represent dimer molecules and the peak at 490 nm represent monomer molecules. In Figure 17-D, the black spectrum is unbound YOYO-1. The peak at 460 nm represents dimer molecules and the peak at 490 nm represents monomer molecules [52].

Dimer molecules have strong influence on absorbance when dye molecules are free in solution. Decreasing on the peak of dimer molecules in the same time increasing on the peak

of monomer molecules indicates that most of dye molecules are bound to CNTs in the monomeric form. Moreover the bathochromic shift proves the noncovalent interactions between dye molecules and CNTs.

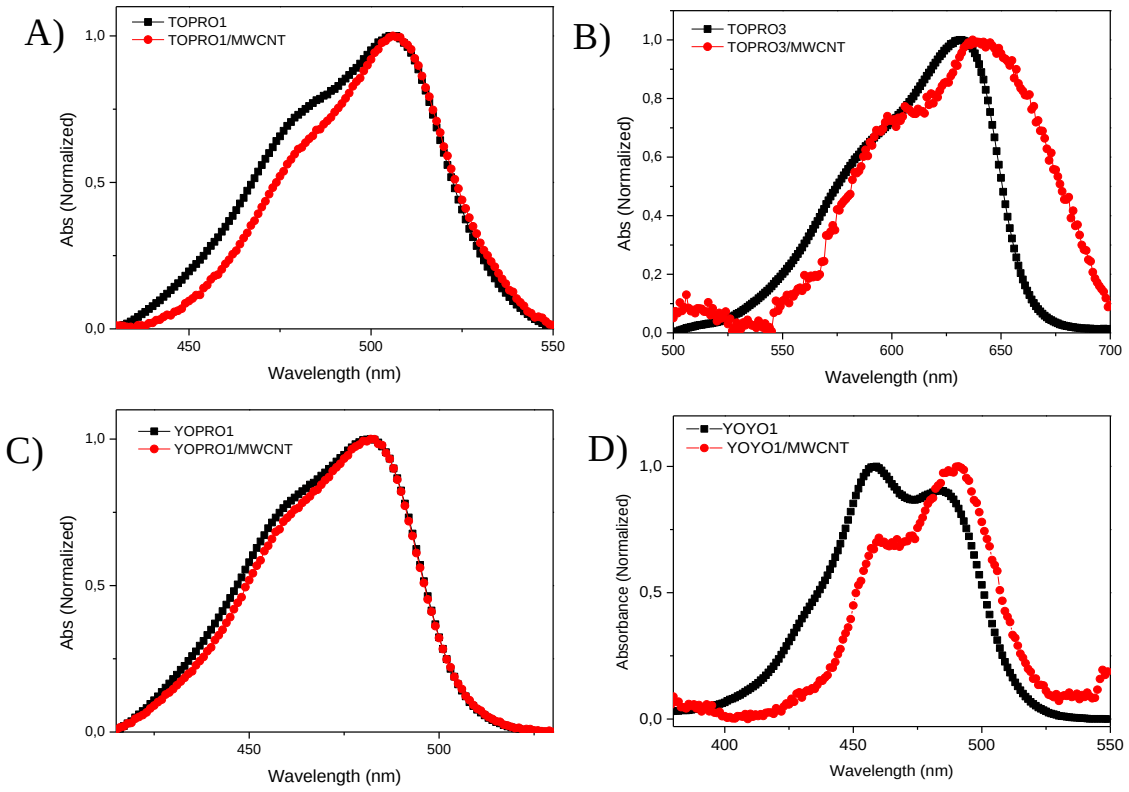

Figure 17 The absorbance spectra of comparison of (A) TO-PRO-1 and TO-PRO-1/MWCNT dispersion (B) TO-PRO-3 and TO-PRO-3/MWCNT dispersion (C) YO-PRO-1 and YO-PRO-1/MWCNT dispersion (D) YOYO-1 and YOYO-1/MWCNT dispersion.

3.4 Fluorescence Spectroscopy

The fluorescence spectroscopy was used to check if dispersed dye/CNT light absorbing system is also fluorescent. But the fluorescence of dyes did not increase as expected (Figure 18). The possible reason is that dye molecules and CNTs might be so close that the dye fluorescence was quenched probably due to electron or energy transfer.

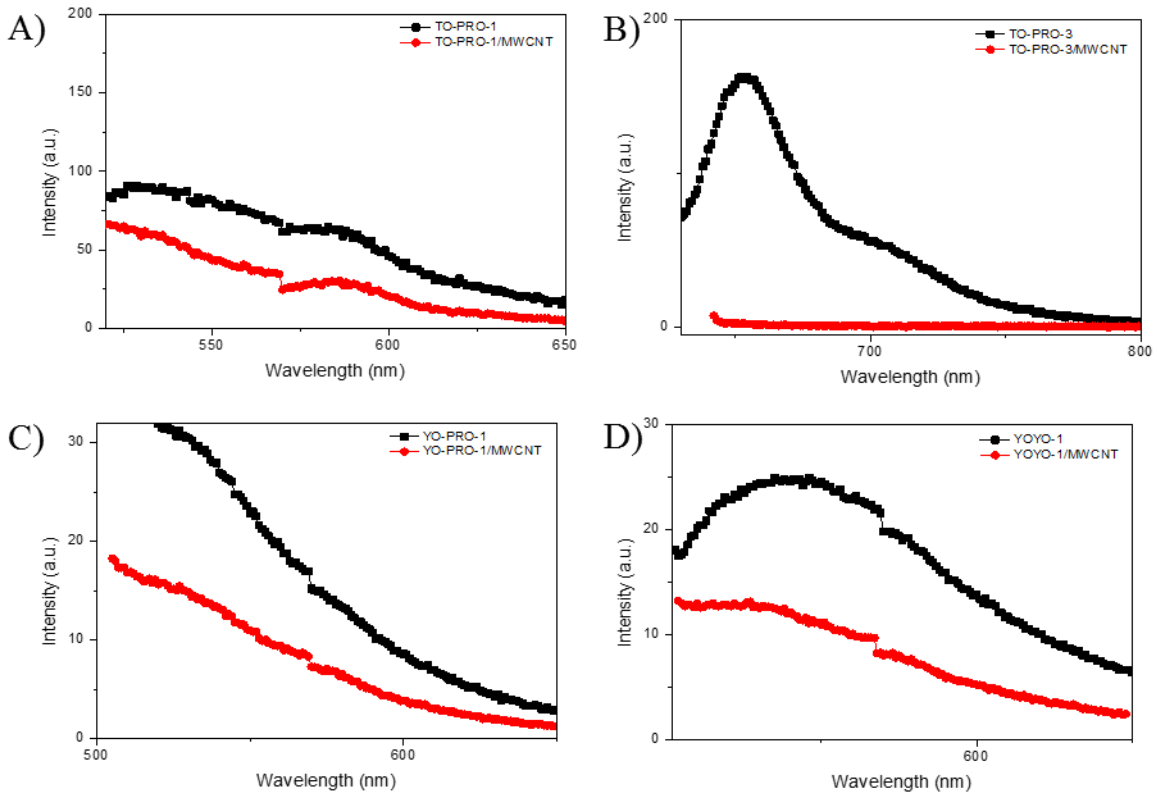

Figure 18 The fluorescence spectra of (A) TO-PRO-1 and TO-PRO-1/MWCNT dispersion (B) TO-PRO-3 and TO-PRO-3/MWCNT dispersion (C) YO-PRO-1 and YO-PRO-1/MWCNT dispersion (D) YOYO-1 and YOYO-1/MWCNT dispersion.

4 Conclusion

In this chapter, decorating CNTs with asymmetrical cyanine dyes was studied. First, interactions between one type of asymmetrical cyanine dye and MWCNT, DWCNT and SWCNT were studied. Second, interactions between asymmetrical cyanine dyes and MWCNT were studied. Dispersion studies proved noncovalent interactions between asymmetrical cyanine dyes and CNTs qualitatively. Furthermore, the upshift at G' band at Raman spectrum and the shift at absorbance peaks of asymmetrical cyanine dyes demonstrated noncovalent interactions quantitatively. Although asymmetrical cyanine dyes bound to CNTs, the fluorescence intensity of the final nanostructure did not increase.

While the method applied did not prove to be an effective method for the fluorescent labeling of CNTs, it resulted in light absorbing nanoarrays. These nanoarrays can be tuned in terms

of the absorbance wavelength by using dye molecules of different spectral properties. We believe that these CNT/dye nanohybrids have large potential as photoactive materials. They can be potentially applied as photothermal materials that can convert the applied light irradiation into heat. Further studies should be conducted to investigate the properties of CNT/asymmetrical cyanine nanohybrids as photoactive materials.

CHAPTER 3 INVESTIGATION OF INTERACTIONS BETWEEN SWCNT/DNA AND ASYMMETRICAL CYANINE DYES

1. Introduction

As a solution to the fluorescence quenching problem presented in the previous chapter we hypothesized that CNTs wrapped with single stranded DNA (ssDNA) could be a better template for the fluorescent activation of the asymmetrical cyanine dyes to fix the problem of fluorescence quenching and achieve fluorescence enhancement of dyes upon binding (Figure 19). It is already known that single stranded DNA (ssDNA) and single walled carbon nanotubes can bind to form a charged hybrid system [53]. Moreover, the fluorescence of asymmetrical cyanine dyes is quenched when they are free in solution. On the other hand when they are in a restrictive environment such as between the base pairs of double stranded DNA, their fluorescence intensity increases several fold. Due to this unique property, cyanine dyes are widely used as DNA intercalators for the labeling and detection of DNA [42]. For this reason, SWCNT/DNA hybrids were prepared and their interactions with asymmetrical cyanine dyes were investigated.

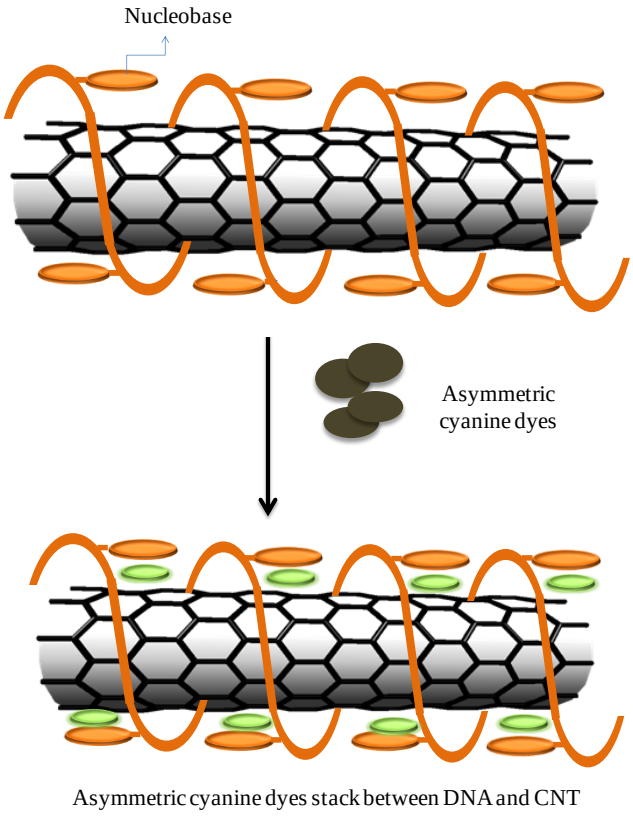

Figure 19 Schematic for the fluorescent labeling of ssDNA/SWCNT scaffold.

2 Materials and Methods

2.1 Materials

Asymmetrical cyanine dyes YO-PRO-1 (Y3603), TO-PRO-1 (T3602), YOYO-1 (Y3601), and TO-PRO-3 (T3605) were purchased from Life Technologies (Figure 10). TO was purchased from Sigma Aldrich. CNTs were purchased from Cheap Tubes Inc. in the form of dry powder. The purity of SWCNTs declared by the supplier is >99%. The outer diameter of SWCNTs as stated by the supplier is 1-2 nm. The length of SWCNTs as specified by the supplier is 3-30 nm. ssDNA composed of 20 Guanines ($Poly(G)_{20}$), 20 Cytosines ($Poly(C)_{20}$), 20 Adenines ($Poly(A)_{20}$), 20 Thymines ($Poly(T)_{20}$) and 37 random bases (Figure 20) were synthesized by Sentromer DNA Technologies, Istanbul, Turkey. Figure 19 shows the structures of DNA bases. Centrifugal filter devices with a 30 kDa cut-off membrane (Microcon-30 kDa) were purchased from Millipore.

Poly(G_{20})= 5’-GGG GGG GGG GGG GGG GGG GG-3’

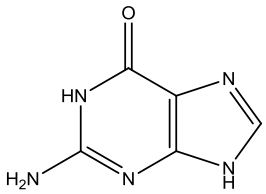

Poly(C_{20})= 5’-CCC CCC CCC CCC CCC CCC CC-3’

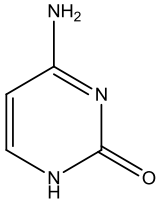

Poly(A_{20})= 5’-AAA AAA AAA AAA AAA AAA AA-3’

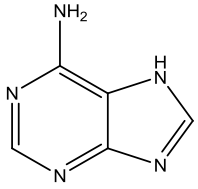

Poly(T_{20})= 5’-TTT TTT TTT TTT TTT TTT TT-3’

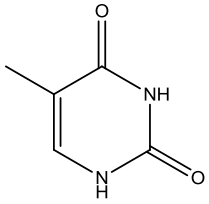

3WJ-S3-T= 5’-TTT TTT TTT TTT TCC GGT CAA CTC TTCTCG CCACCT G-3’

Figure 20 Structures of DNA bases and sequences of ssDNA.

2.2 Methods

2.2.1 Experimental

Preparation of ssDNA/SWCNT Nanostructures:

A 500 μL of a dispersal solution containing 0.1 mg/mL SWCNT and 10 μM ssDNA in 0.1 M NaCl was prepared. The dispersal solution was sonicated with a microprobe for 45 min with 2 seconds pulse-on and 5 seconds pulse-off time in ice. The dispersion was ultracentrifuged at 14,000 rpm for 10 min and the black supernatant was transferred into a clean eppendorf tube.

$MgCl_2$ precipitation procedure: 30mM $MgCl_2$ was added into the dispersion and centrifuged 10 min at 14krpm. CNT/DNA system was centrifuged and the supernatant which had free DNA was separated. The black pellet composed of ssDNA/SWCNT conjugates was

redispersed in 0.5X TBE buffer (44.5 Mm Tris, 1mM EDTA, 44.5Mm Boric acid, pH 8.0) containing 30mM NaCl and 10mM extra EDTA to complex with residual Mg^{+2}.

Preparation of ssDNA/SWCNT/dye nanohybrids with one step sonication:

A dispersal solution containing 0.1 mg/mL SWCNT, 30 μM dye and 10 μM $Poly(G)_{20}$ was prepared in water. The solution was ultrasonicated with a microprobe for 30 minutes with a 2 seconds pulse-on and 5 seconds pulse-off time in ice. The resulting dispersion was centrifuged at 14,000 rpm for 10 minutes and the supernatant was transferred into a clean eppendorf tube. The ssDNA/SWCNT/dye nanohybrid was filtered by using a Microcon centrifugal filter device with a 30,000 Da cut-off membrane to remove unbound ssDNA, unbound dye and ssDNA/dye conjugates.

Preparation of dsDNA:

A solution containing 1μM $Poly(G)_{20}$ and 1μM $Poly(C)_{20}$ was prepared in TE buffer. The mixture was heated until 95^{o}C and incubated 5 min at this temperature in the heating block. As soon as taking out the mixture from the heating block, it was placed in an ice bucket for 30 min.

Preparation of 2% Agarose Gel:

1 mg of agarose was mixed with 50 mL of TBE buffer and microwaved until it melted. The gel was run at 150 V, 20 min. Gel red was used to visualize free DNA.

2.2.1 Characterizations

For Raman Spectroscopy analysis 10 μL drops of 10 μM of ssDNA and 0.1 mg/mL of CNT dispersion was dried on silicon wafers and measurements were made on a Renishaw in Via Reflex Raman Spectrometer set with a 532 nm laser.

Absorbance measurements were made on a Cary 5000 Spectrophotometer. Samples were transferred into 500 μl quartz cuvettes and scanned 200-800 nm.

Fluorescence analysis was made on a Cary Eclipse Fluorescence Spectrophotometer. Measurements were made in 500 μl quartz cuvettes. Dyes and Dye/SWCNT conjugates were excited at the following wavelengths: TO: 490nm, TO-PRO-1: 490nm, TO-PRO-3: 620nm, YO-PRO-1: 480nm, YOYO-1: 480nm. The bandwidth for excitation and emission was 5nm.

The thermal stability measurements were completed on the Cary Eclipse spectrophotometer equipped with a Peltier-Thermostatted cell holder. The samples were heated from 25ºC to 90ºC with a rate of 1ºC/min, incubated for 5 minutes at 90ºC and cooled back to 30ºC with the same rate as the fluorescence at $\lambda_{max,e}$, is monitored.

Microscopy samples were prepared on glass slides by dropping 10 μL of the nanohybrid to be visualized on a glass slide. Confocal Laser Scanning Microscopy images were acquired with a Carl-Zeiss LSM 710 confocal microscope equipped with a Plan-Apochromat 63x/1.40 Oil objective. CNTs were excited with a 488 nm laser and images were collected using a 493nm-639 nm filter. DIC images were obtained with excitation of 405 nm laser.

Scanning Electron Microscopy (SEM) analysis were performed using JEOL JIB-4501 SEM.

Transmission Electron Microscopy (TEM) analysis were carried out utilizing JEOL JEM-ARM200CFEG UHR-TEM

3 Results and Discussion

3.1 Preparation of ssDNA/SWCNT template

ssDNA/SWCNT template was prepared by the ultrasonication of solid SWCNT in an aqueous solution of ssDNA. Firstly, 500 μL of 10 μM random ssDNA in 0.1 mM NaCl was sonicated with 0.1 mg/mL of SWCNT followed by centrifugation to remove undispersed SWCNTs. The resulting dispersion was treated with $MgCl_2$ with the aim of selectively precipitating the SWCNT/ssDNA and removing the unbound ssDNA. After the removal of the unbound ssDNA, SWCNT/ssDNA pellet was rehybridized with a buffer that contains EDTA and SWCNT/ssDNA dispersion that does not contain any unbound ssDNA was obtained. Figure 21-A shows a picture of the resulting dispersion. SWCNTs were finely dispersed in the presence of ssDNA. When the same amount of CNTs was ultrasonicated with the buffer as a control, dispersion was not observed (Figure 21-B) indicating that the dispersion shown in Figure 21-A is obtained due to the binding ssDNA onto CNTs.

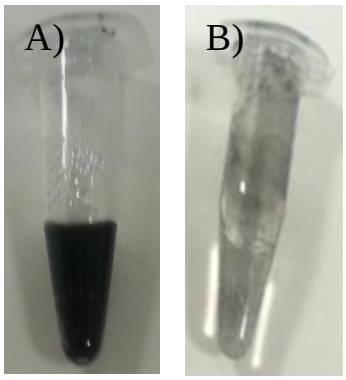

Figure 21 Comparison of (A) 10uM ssDNA sonicated with 0.1mg/ml SWCNT in 0.1M NaCl and (B) 0.1mg/ml SWCNT sonicated in 0.1 M NaCl

Agarose gel electrophoresis was utilized to show whether the free DNA was successfully removed from the dispersion. The first well in Figure 22 contains free ssDNA and second well contains ssDNA/CNT dispersion. In Agarose gel electrophoresis, smaller molecules travel faster than larger molecules. Since ssDNA is smaller than the hybrid structure, it migrated farther. Moreover, the second well did not have the free ssDNA trace as the first well. The agarose gel electrophoresis proved that all free DNA was removed from the dispersion.

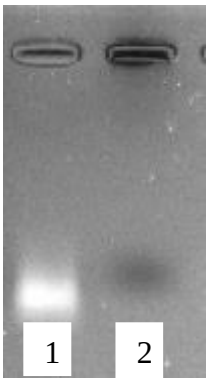

Figure 22 Agarose gel image of ssDNA (1) and ssDNA/CNT dispersion (2).

3.2 Raman Spectroscopy

Noncovalent interactions between DNA and CNT were examined by Raman Spectroscopy. Figure 23 presents the spectrum of pristine SWCNTs in comparison to ssDNA/SWCNT dispersion. While the G band of pristine SWCNT is at 1584 cm^{-1}, this band exhibits an upshift to 1592 cm^{-1} when the SWCNT is bound to ssDNA. This shift demonstrates the presence of

noncovalent binding interactions between ssDNA and SWCNT resulting in changes in electronic structure of SWCNTs.

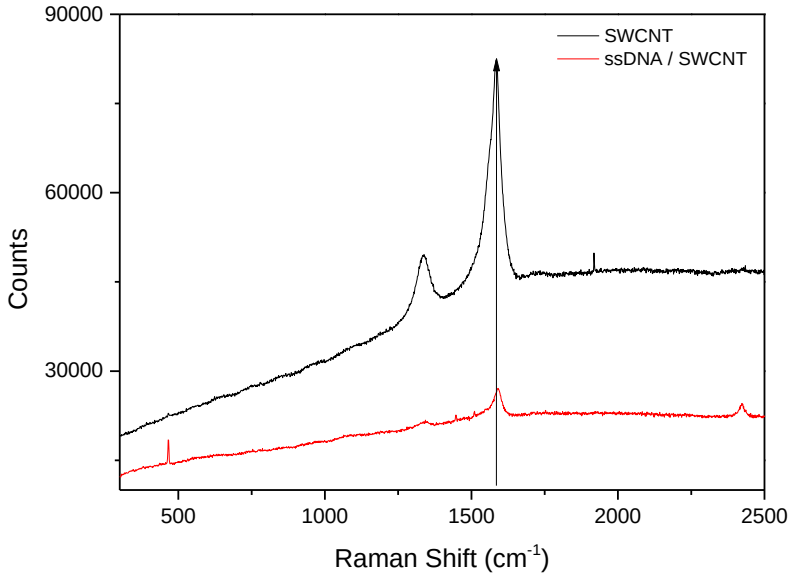

Figure 23 Raman spectra of SWCNT (black) and ssDNA/SWCNT dispersion (red).

3.3 Binding of Asymmetrical Cyanine Dyes onto the ssDNA/CNT Template

To investigate the interactions between ssDNA/CNT template and asymmetrical cyanine dyes, 3 different methods were used.

- Titration of ssDNA/SWCNT scaffold into dye solutions
- Titration of dye solutions into ssDNA/SWCNT scaffold
- One-step Preparation of ssDNA/SWCNT/dye nanohybrids

3.3.1 Titration of ssDNA/SWCNT scaffold into dye solutions

In this method, aliquots of ssDNA/SWCNT were added into the 1 μM aqueous solution of asymmetrical cyanine dye solution (Figure 24). The fluorescence intensity of the mixture was measured after each addition to monitor the increase of the fluorescence and to determine the point at which the fluorescence is saturated.

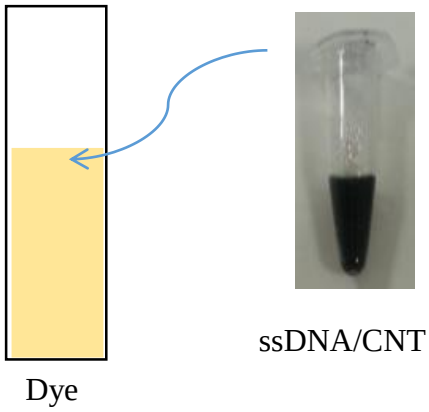

Figure 24 Illustration of the first method of titration studies.

3.3.1.1 Fluorescence Spectroscopy

Fluorescence spectrophotometer was used for measuring fluorescence intensity of dyes and titration of dyes and ssDNA/CNT systems. Firstly, 3WJ-S3-T/SWCNT scaffold was analyzed to demonstrate whether the template and the dye would have interactions. 1µM asymmetrical dye solution was titrated with ssDNA/SWCNT scaffold. Figure 25-A shows the fluorescence spectrum of unbound YO-PRO-1 (black) in comparison to the spectrum of the same dye saturated with ssDNA/SWCNT hybrid (red). As it is seen in Figure 25-A, when asymmetrical cyanine dye molecules are free in a solution, they are quenched and show background fluorescence. Their fluorescence was increased by addition of ssDNA/SWCNT template. As we hypothesized ssDNA/SWCNT acted as an appropriate template for the binding and fluorescence activation of the asymmetrical cyanine dye. Titrations of ssDNA/SWCNT template into dye solutions were repeated with asymmetrical cyanine dyes of different structures to investigate the effect of the size and charge of the dye on its binding to ssDNA/SWCNT. Figure 25 exhibits that all of the dyes were able to bind to the ssDNA/SWCNT with an increased quantum yield as seen by the increase of the fluorescence intensity. This result demonstrates that the ssDNA/SWCNT template can accommodate asymmetrical cyanine dyes of different structures and provide an appropriate medium for fluorescence enhancement. Quantitative analysis of different binding affinities of these dyes was made in the following sections of this thesis.

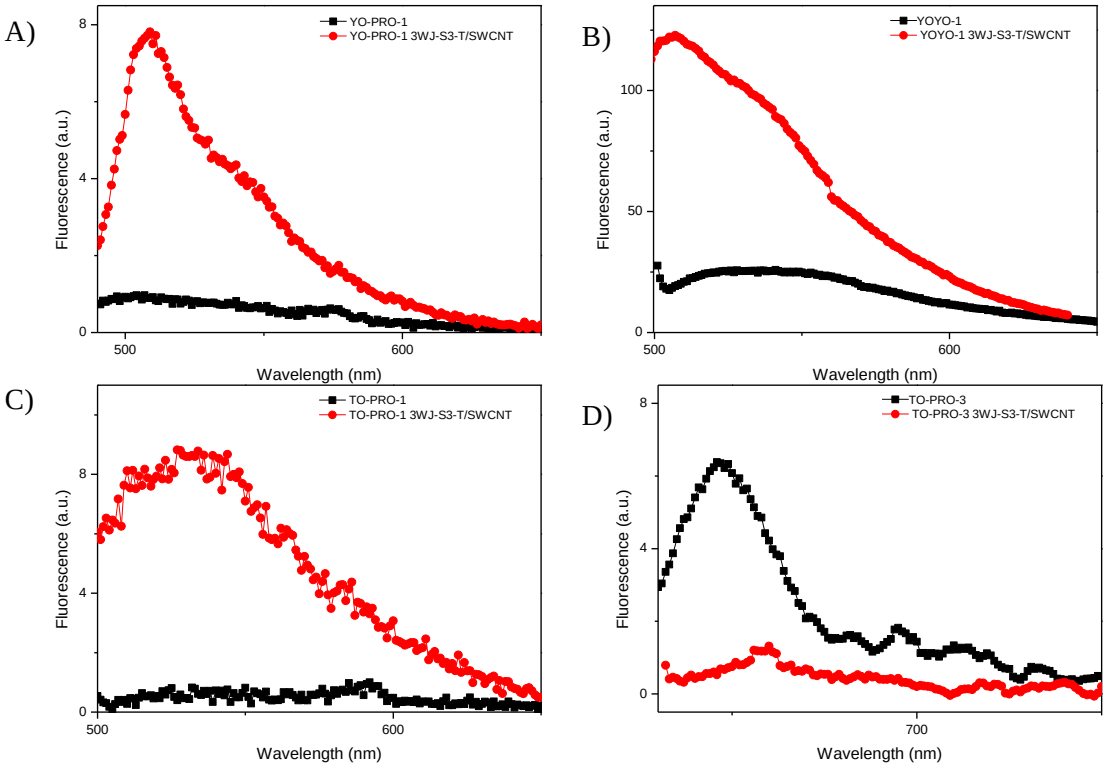

Figure 25 The comparison of fluorescence intensity of asymmetrical cyanine dyes ssDNA/SWCNT scaffold (A) YO-PRO-1 and YO-PRO-1 ssDNA/SWCNT titration (B) YOYO-1 and YOYO-1 ssDNA/SWCNT titration (C) TO-PRO-1 and TO-PRO-1 ssDNA/SWCNT titration (D) TO-PRO-3 and TO-PRO-3 ssDNA/SWCNT titration.

Moreover, to investigate which DNA base leads to a higher suitable fluorescence enhancement with cyanine dyes, YO-PRO-1 was titrated with Poly$(G)_{20}$/SWCNT scaffold, Poly$(A)_{20}$/SWCNT scaffold, Poly$(C)_{20}$/SWCNT scaffold and Poly$(T)_{20}$/SWCNT scaffold.

Figure 26 shows that the scaffold prepared with Poly-Guanine has stronger non-covalent interactions with asymmetrical cyanine dyes as seen by the higher fold increase of the fluorescence intensity upon binding to the YO-PRO-1 dye. The fluorescence enhancement upon binding to the template decreases in sequence of G>A>C>T which means Poly$(G)_{20}$/SWCNT template provides the optimum binding environment for dyes. The reason of this ranking could be the solvent effect due to hydrogen bonding between the solvent and bases [54]. According to Zeng DNA bases have self-stacking when they are dissolved in water. Therefore their binding energy is different from each other. [22]. Hence

their binding energy might be affected by the type of solvent such as different salty aqueous solutions.

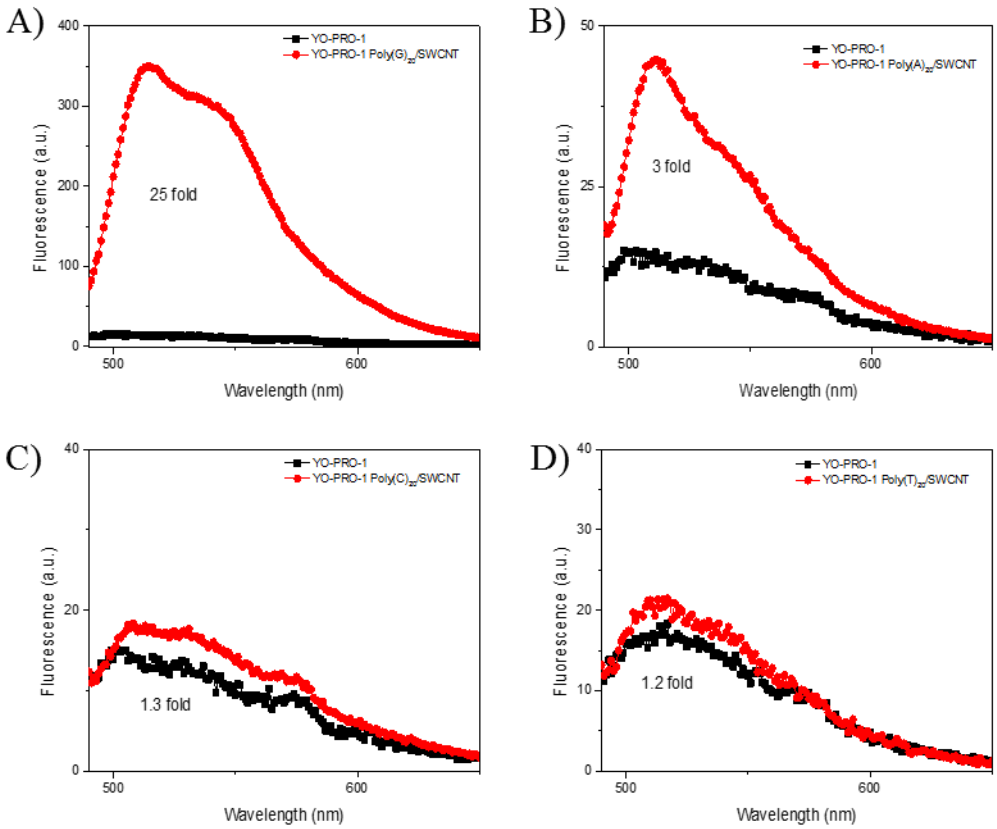

Figure 26 The fluorescence spectra (A) YO-PRO-1 and YO-PRO-1 Poly(G)$_{20}$/SWCNT titration (B) YO-PRO-1 and YO-PRO-1 Poly(A)$_{20}$/SWCNT titration (C) YO-PRO-1 and YO-PRO-1 Poly(C)$_{20}$/SWCNT titration (D) YO-PRO-1 and YO-PRO-1 Poly(T)$_{20}$/SWCNT titration.

Due to the fact that Poly(G)$_{20}$/SWCNT provided the environment that lead to the highest fluorescence increase upon binding of the dye molecule, this template was utilized for the rest of the studies.

Figure 27-A shows how unbound YO-PRO-1 that was not fluorescent turned fluorescent during titration, after a certain amount of Poly(G)$_{20}$/SWCNT template was added.

Figure 27-B represents the corresponding titration curve. The titration curve indicates that fluorescence intensity of YO-PRO-1 increases as more Poly(G)$_{20}$/SWCNT was added up to

a point of saturation at which all of the dye molecules in the cuvette were bound to the template. The ratio of concentration of DNA bases to the concentration of dye molecules at the saturation point determines that there is approximately 1 dye molecule for every 4 DNA bases on the Poly(G)$_{20}$/SWCNT template.

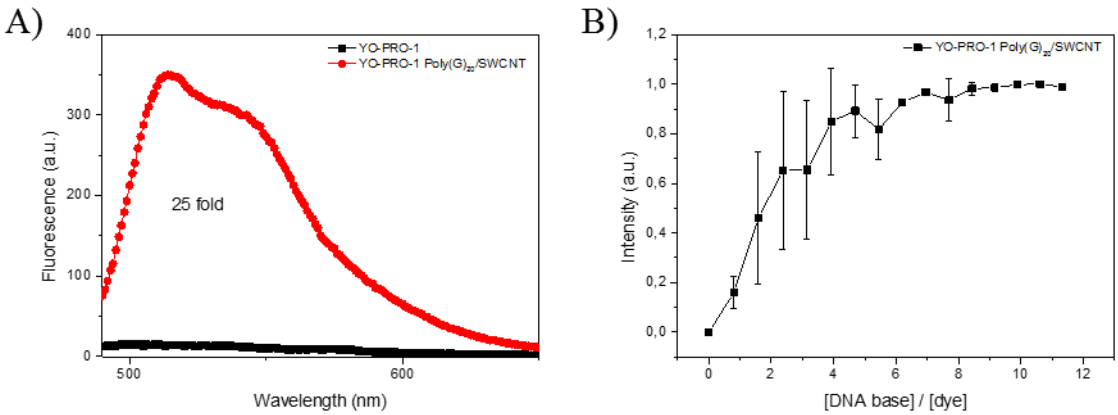

Figure 27 (A) The fluorescence spectra of saturated YO-PRO-1 Poly(G)20/SWCNT system (b) The titration curve of YO-PRO-1 Poly(G)20/SWCNT system.

4.3.1.2 Characterization of Binding Interactions between ssDNA/SWCNT and asymmetrical cyanine dyes with UV-vis Spectroscopy

UV-vis spectrophotometer was utilized for measuring absorbance of ssDNA/SWCNT/dye systems. Figure 28-A shows the UV-vis absorbance analysis of the titration of Poly(G)$_{20}$/SWCNT dispersion into 1uM YO-PRO-1 at the saturation point. The black spectrum is unbound dye which has maximum absorbance at 480 nm and a weaker band at 460 nm, but the situation is changed when Poly(G)$_{20}$/SWCNT dispersion was added into the dye solution. The red spectrum was obtained when YO-PRO-1 was saturated with Poly(G)$_{20}$/SWCNT . Addition of Poly(G)$_{20}$/SWCNT dispersion caused a bathochromic shift. Moreover, the change in absorbance intensity and shape of peaks indicate that ssDNA/SWCNT template interact with asymmetrical cyanine dyes and provides an exclusive environment for dye molecules. As a control to rule out the binding of the dye to ssDNA only, instead of the ssDNA/SWCNT template, ssDNA was added into the YO-PRO-1 solution and the absorbance spectrum was obtained at the saturation point (pink spectrum). The fact that different shapes of spectra were obtained in both cases indicates that YO-PRO-

1 molecules are in a completely different electronic environment when bound to ssDNA/SWCNT template than ssDNA only. Thus, a trimolecular nanohybrid structure composed of ssDNA, SWCNT and dye molecules were obtained. Same results in terms of the bathochromic shifts were observed with YOYO-1 Poly$(G)_{20}$/SWCNT, TO-PRO-1 Poly$(G)_{20}$/SWCNT and TO-PRO-3 Poly$(G)_{20}$/SWCNT indicating that all of these dyes can actually bind to the Poly$(G)_{20}$/SWCNT template resulting in changes of their electronic environment All spectra in Figure 28 were corrected for ssDNA/SWCNT hybrid absorbance in this wavelength range to monitor bathochromic shift easier.

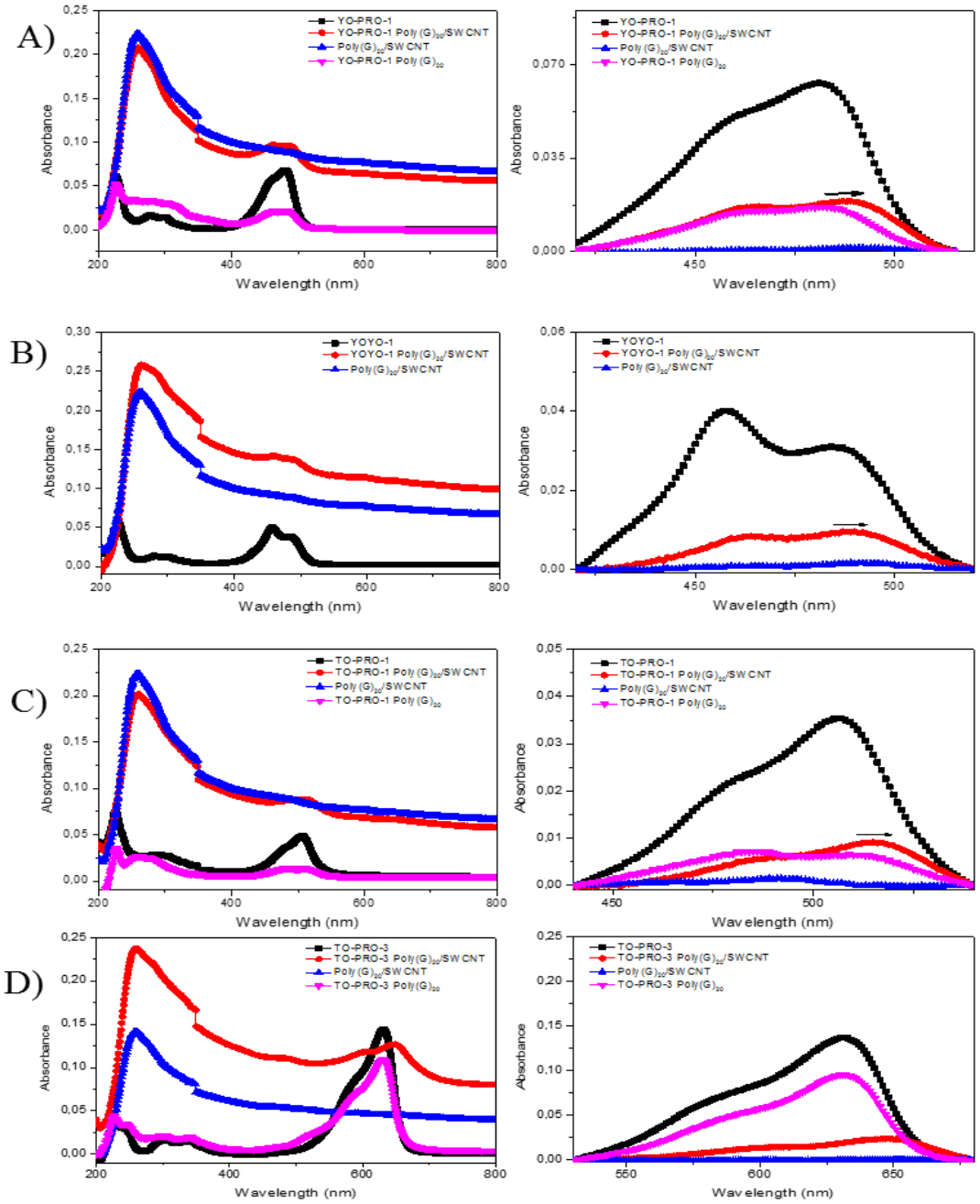

Figure 28 UV-vis spectra of (A) YO-PRO-1 (black), YO-PRO-1 Poly(G)$_{20}$/SWCNT system (red), Poly(G)$_{20}$/SWCNT (blue) and YO-PRO-1 Poly(G)$_{20}$ system (pink). (B) YOYO-1, YOYO-1 Poly(G)$_{20}$/SWCNT system and Poly(G)$_{20}$. (C) TO-PRO-1, TO-PRO-1 Poly(G)$_{20}$/SWCNT system, Poly(G)$_{20}$/SWCNT and TO-PRO-1 Poly(G)$_{20}$ system. (D) TO-PRO-3, TO-PRO-3 Poly(G)$_{20}$/SWCNT system, Poly(G)$_{20}$/SWCNT and TO-PRO-3 Poly(G)$_{20}$ system.

3.3.2 Titration of dye solutions into ssDNA/SWCNT scaffold

Second method used to prepare ssDNA/SWCNT/dye nanohybrids was the titration of asymmetrical cyanine dyes into a solution of ssDNA/SWCNT hybrids (Figure 29). Aliquots of 100 µM asymmetrical cyanine dye were titrated into 0.25 µM ssDNA/CNT template as the fluorescence intensity was monitored. Resulting mixtures at the saturation point were examined by fluorescence spectroscopy, fluorescent based thermal analysis and UV-vis spectroscopy.

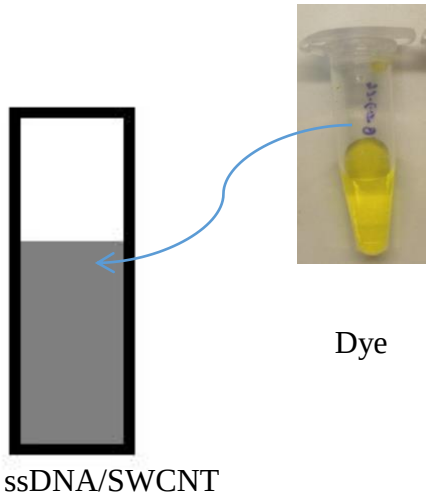

Figure 29 Illustration of the second method to prepare ssDNA/SWCNT/dye nanohybrids: Titration of dye into ssDNA/SWCNT template

3.3.2.1 Fluorescence Spectroscopy

Fluorescence spectrophotometer was used for measuring fluorescence intensity of titration of dyes into ssDNA/SWCNT template. In Figure 30-A, the black spectrum is Poly$(G)_{20}$/SWCNT template, the red spectrum is the spectrum obtained at the saturation point and the blue spectrum is unbound YOPRO1. Non-fluorescent ssDNA/CNT template becomes highly fluorescent after the titration with the cyanine dye.

Figure 30-B demonstrates the corresponding titration curve. The titration curve indicates that the fluorescence intensity increases as more dye molecules were added into a point of fluorescence saturation at which the entire ssDNA/SWCNT template in the cuvette was bound to the dyes added. The ratio of DNA base concentration to the concentration of dye molecules at the saturation point determines that there is approximately 1 dye molecule for

every 4 bases. The same stoichiometry of binding was obtained when the nanohybrids were prepared with a different method as shown in the previous section of this thesis. This fact demonstrates that Poly(G)$_{20}$/SWCNT template acts as a predefined scaffold for the stoichiometric binding of YO-PRO-1 molecules instead of being a random self-assembly.

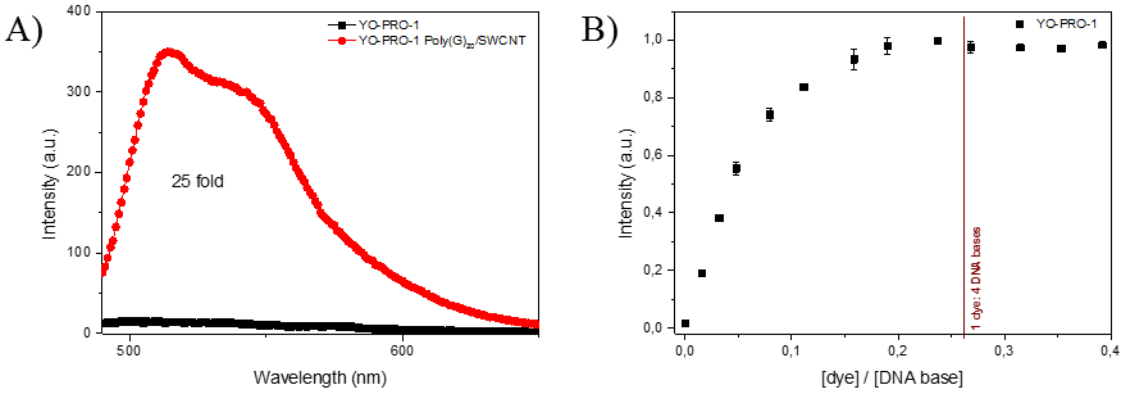

Figure 30 (A) The fluorescence spectra of saturated Poly(G)$_{20}$/SWCNT YO-PRO-1 system. (B) The titration curve of Poly(G)$_{20}$/SWCNT YO-PRO-1 system.

As it is seen in the Figure 31, the non-fluorescent Poly(G)$_{20}$/SWCNT template became fluorescent, after titrations with YOYO-1, TO-PRO-1 and TO. On the other hand, in Figure 31, the black spectrum is Poly(G)$_{20}$/SWCNT template, the red spectrum is Poly(G)$_{20}$/SWCNT titrated with TO-PRO-3 and the blue spectrum is the same amount of TO-PRO-3 which was used in titration. The bathochromic shift indicates that TO-PRO-3 has noncovalent binding with DNA/CNT template. But the fluorescence did not increase as expected. The reason is that TO-PRO-3 has three carbon atoms in the methine bridge therefore due to their larger size dye molecules may not fit between CNT and DNA template from certain distance to become fluorescent. Thus the dye fluorescence was quenched due to electron or energy transfer.

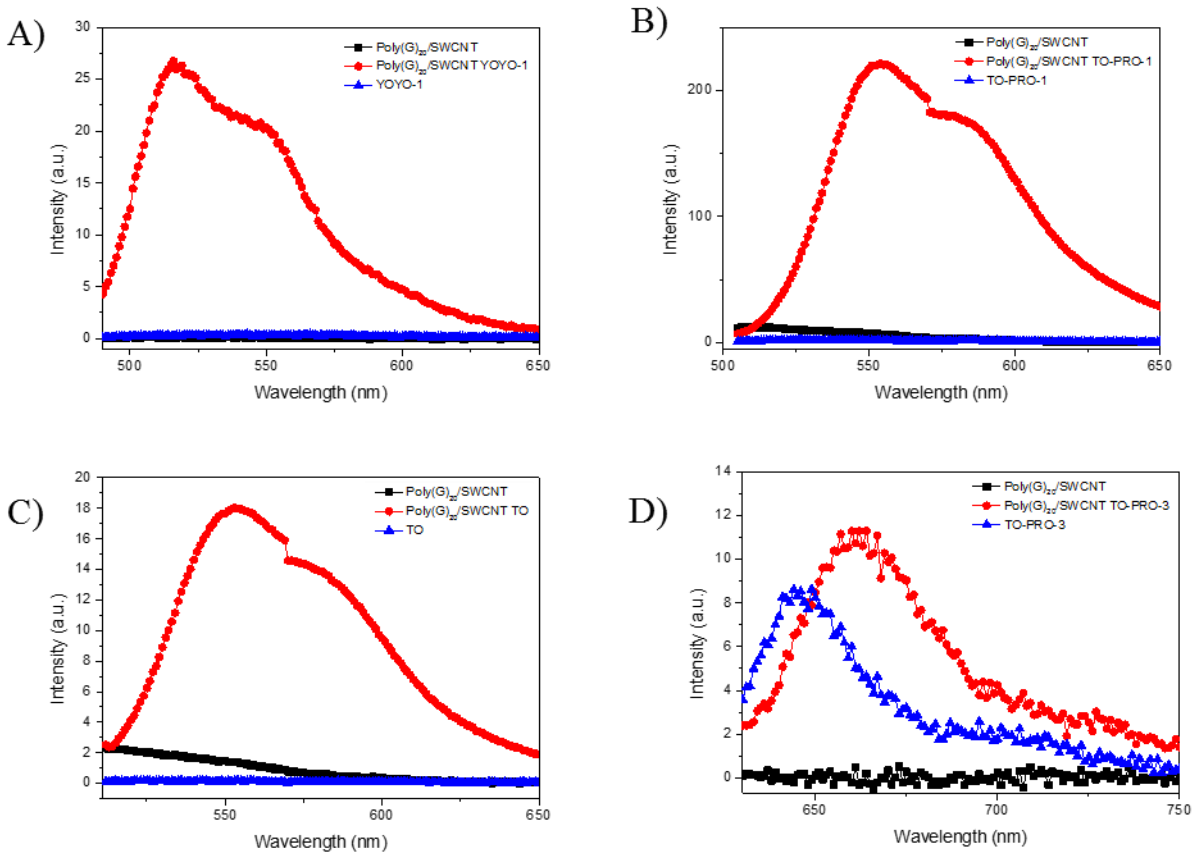

Figure 31 The fluorescence spectra of saturated (A) Poly(G)$_{20}$/SWCNT YOYO-1 system. (B) Poly(G)$_{20}$/SWCNT TO-PRO-1 (C) Poly(G)$_{20}$/SWCNT TO (D) Poly(G)$_{20}$/SWCNT TO-PRO-3

In

Figure 32 titration curves of asymmetrical cyanine dyes was compared. The red spectrum is YOYO-1, black spectrum is YO-PRO-1, blue spectrum is TO-PRO-1 and pink spectrum is TO titrated into ssDNA/SWCNT template. The reason of the linear increase of titration curves is that the dye molecules bind to available binding sites on the ssDNA/SWCNT scaffold. For YO-PRO-1, TO-PRO-1, there is approximately 1 dye molecule for every 4 DNA bases. The length of YO-PRO-1 and TO-PRO-1 is nearly same. Thus, their binding affinity with ssDNA/SWCNT template is similar. When the same titration was completed with YOYO-1 which is dimeric form of YO-PRO-1, dye to ssDNA base ratio was doubled when it was compared with YO-PRO-1. There is 1 dye molecule for every 8 DNA bases. On the other hand for TO, there is nearly 1 dye molecule for every 2 DNA bases and the binding affinity of TO is weaker than the binding affinity of TO-PRO-1 The reason of the difference

between TO and TO-PRO-1, the cationic electron structure of TO-PRO-1 possibly provides better binding affinity because of anionic structure of ssDNA. This result further confirms the quantitative binding of dye molecules. Moreover, interactions between ssDNA/CNT template and dye molecules present similar behavior as the intercalation of the same dyes between base pairs of double stranded DNA.

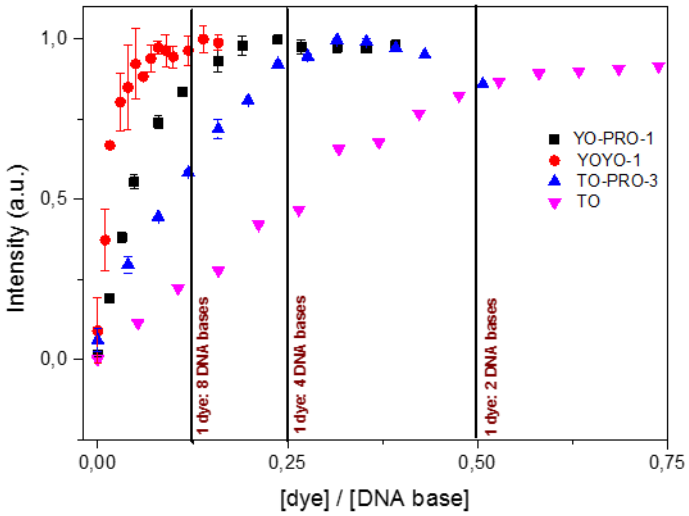

Figure 32 The comparison of the titration curves of asymmetrical cyanine dyes.

3.3.2.2 Fluorescent Based Thermal Analysis of ssDNA/SWCNT/dye nanohybrids

Fluorescence spectrophotometer was used to examine thermal stability of ssDNA/SWCNT/Dye nanohybrids. When the titration reached the saturation point, the thermal analysis was started. The sample was heated from 25°C to 90°C at the rate of 1°C/min followed by a cooling cycle from 90°C to 25°C at the same rate. In Figure 33-A the black spectrum is the heating curve for Poly$(G)_{20}$/SWCNT /YO-PRO-1 nanohybrid. The fluorescence of the system was stable until 70°C. After 70°C, the intensity started to decrease. Possible reason of this decrease on intensity is that the noncovalent interactions between the dye and the template and also DNA and CNT are broken. Fluorescence intensity started to increase with the cooling cycle as demonstrated with the red spectrum. The cooling cycle did not duplicate the heating cycle and the fluorescence intensity at the end of the cycle

was higher than the initial intensity illustrating that the same nanohybrid was not able to self-assemble again, instead different fluorescent structures have formed. Our assumption is that at high temperatures the ssDNA/SWCNT template dissociates irreversibly leading to the binding of the free dye molecules to the free ssDNA during the cooling cycle. This assumption was supported by the appearance of the solutions at the end of the thermal cycle. Before the thermal cycle CNTs were well dispersed in the transparent ssDNA/SWCNT/dye hybrid solution whereas at the end of the thermal cycle CNTs became noticeable in the aggregated form (Figure 33-B). The blue and pink spectra belong to control experiment. Same amount of aqueous solution of YO-PRO-1 was analyzed with fluorescent based thermal analysis. This control experiment further proves that the high fluorescence intensity is caused by the presence of a 3-molecular nanostructure.

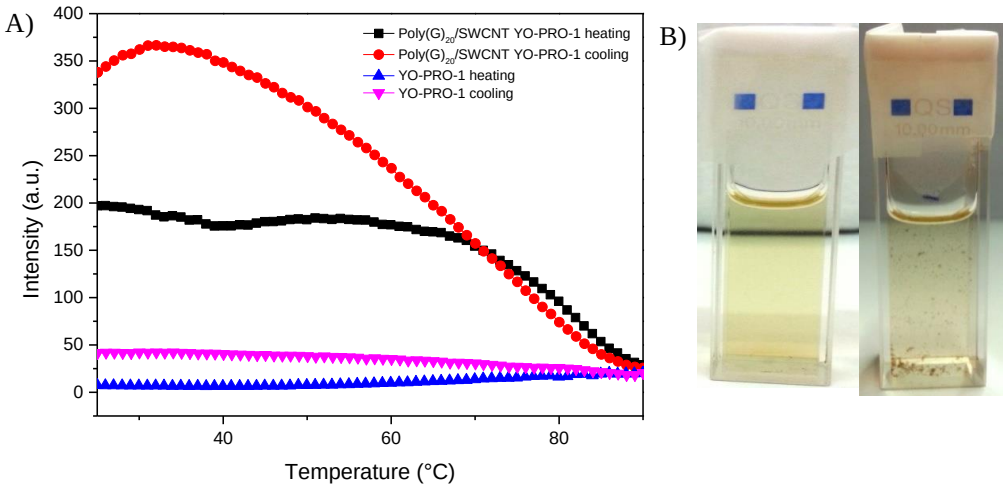

Figure 33 (A) Fluorescence based thermal analysis spectra of YO-PRO-1 (blue-heating, pink-cooling), YO-PRO-1 Poly$(G)_{20}$/SWCNT nanohybrid at the fluorescence emission maximum (black-heating, red-cooling).(B) Poly$(G)_{20}$/SWCNT/YO-PRO-1 before (left) and after (right) thermal analysis

To compare the stability of the ssDNA/SWCNT/dye hybrid structure, same analysis was repeated by using YOYO-1, TO-PRO-1 and TO. Figure 34 illustrates the thermal stability of ssDNA/SWCNT/dye nanohybrids containing different asymmetrical cyanine dyes. Table 2 Dissociation Temperatures of ssDNA/SWCNT/dye hybrid prepared by using different dyes. Table 2 indicates that ssDNA/SWCNT/dye hybrid was dissociated at different temperatures with different dyes. While nanohybrids containing YO-PRO-1, YOYO-1 and TO-PRO-1

started to dissociate approximately at the same temperature, TO dissociate at a lower temperature. YO-PRO-1, YOYO-1 and TO-PRO-1 have an extra cationic charge whereas TO is neutral. The reason of this difference in the stability can be that cationic dyes have higher strength with ssDNA/SWCNT hybrid due to the negatively charged backbone of ssDNA.

Table 2 Dissociation Temperatures of ssDNA/SWCNT/dye hybrid prepared by using different dyes.

Dye	Dissociation Temperature (^{o}C)
YO-PRO-1	59.0 ± 2.0
YOYO-1	59.0 ± 1.0
TO-PRO-1	51.5 ± 0.5
TO	59.5 ± 2.6

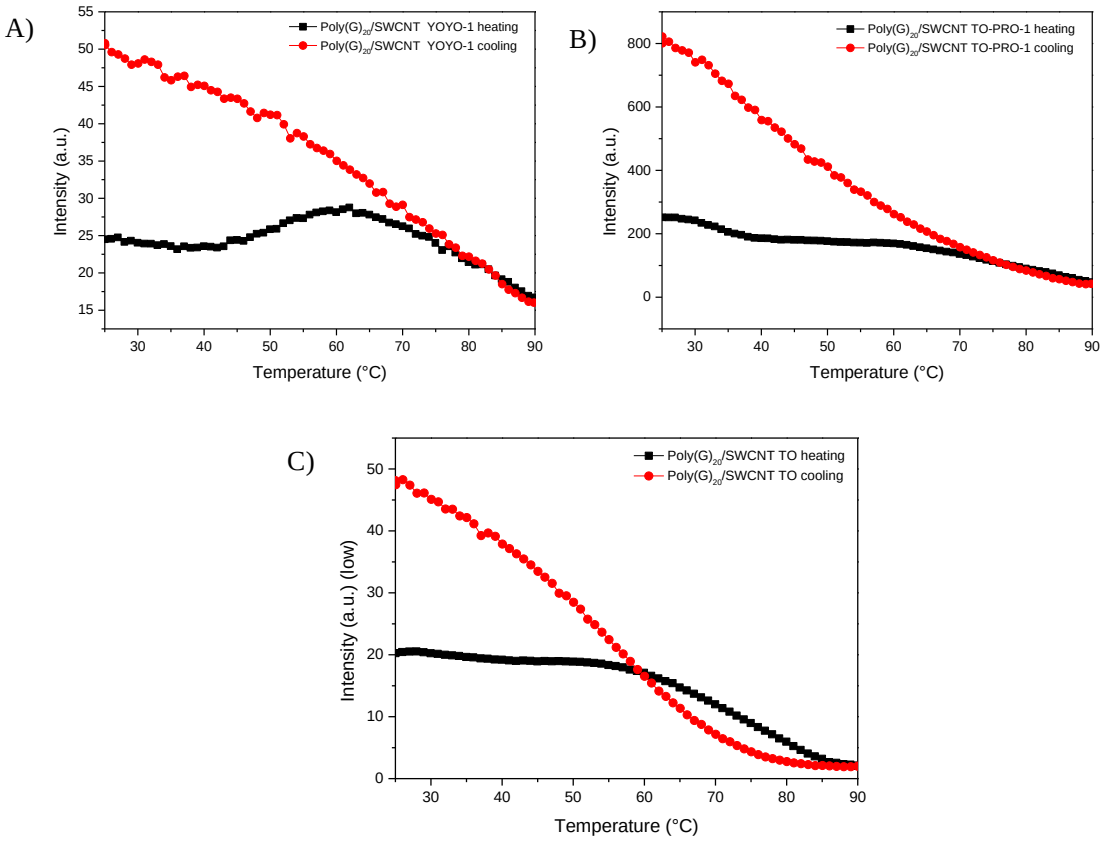

Figure 34 Fluorescence based thermal analysis spectra of (A) Poly(G)$_{20}$/SWCNT/ YOYO-1 nanohybrids (B) Poly(G)$_{20}$/SWCNT/ TO-PRO-1 nanohybrids (C) Poly(G)$_{20}$/SWCNT/ TO nanohybrids.

3.3.2.3 UV-vis Spectroscopy

UV-vis spectrophotometer was utilized for measuring the absorbance of ssDNA/SWCNT/dye nanohybrids before and after the thermal analysis. In Figure 35, to compare the changes in the dye absorbance, spectra were corrected (Figure 35-A) for ssDNA/SWCNT hybrid absorbance in this wavelength range and normalized by dividing all data points by the maximum absorbance (Figure 35-B). The black spectrum represents Poly(G)$_{20}$/SWCNT/YO-PRO-1 absorbance before thermal analysis. The red spectrum is Poly(G)$_{20}$/SWCNT YO-PRO-1 system after thermal analysis. The peak at 460 nm increased after thermal analysis due to increase in dimer molecules. The blue spectrum is the aqueous solution of YO-PRO-1. The UV-vis spectrum indicates that during the thermal cycle ssDNA/SWCNT/dye hybrid structure was broken. This can be another prove that

ssDNA/SWCNT hybrid interacts with dye molecules non-covalently.

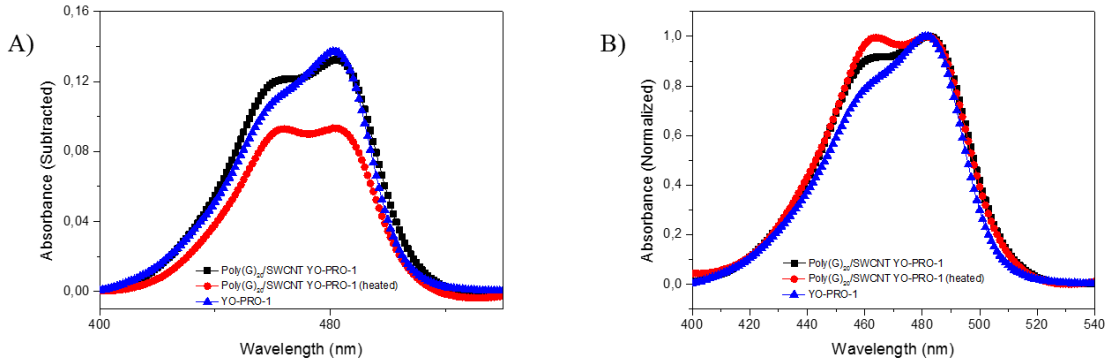

Figure 35 UV-vis spectrum of comparison of Poly(G)$_{20}$/SWCNT/YO-PRO-1 before thermal (black), Poly(G)$_{20}$/SWCNT YO-PRO-1 after thermal (red) and, YO-PRO-1 (blue).

3.4 One-step Preparation of ssDNA/SWCNT/dye nanohybrids

In order to understand whether the order of addition matters for the self-assembly of these nanohybrids we tried mixing all three components together instead of adding dye molecules into a premade ssDNA/CNT scaffold. A dispersal solution containing 10 µM Poly(G)$_{20}$, 30 µM dye and 0.1 mg/ml SWCNT was prepared under ultrasonication. In Figure 38, the first picture is ultrasonicated Poly(G)$_{20}$/SWCNT /YO-PRO-1 which was taken after the removal of undispersed CNTs by ultracentrifugation and the second picture is CNT ultrasonicated with ssDNA in H_2O which was taken after removal of undispersed CNTs. Free ssDNA was removed by the centrifugal filter device with the appropriate cut off membrane that allows separation of unbound dye molecules, unbound ssDNA molecules and also any ssDNA/YOPRO1 hybrids that are not associated with SWCNTs. As can be seen in Figure 36-A ssDNA and YO-PRO-1 molecules together allowed the debundling of SWCNTs and a three-component hybrid nanostructure was self-assembled again. The control experiment where the same amount of ssDNA and SWCNT were sonicated in water resulted in SWCNTs that were not dispersed (Figure 36-B). This result clearly demonstrates the strong dispersing effect dye molecules on SWCNTs and a trimolecular nanohybrid was prepared.

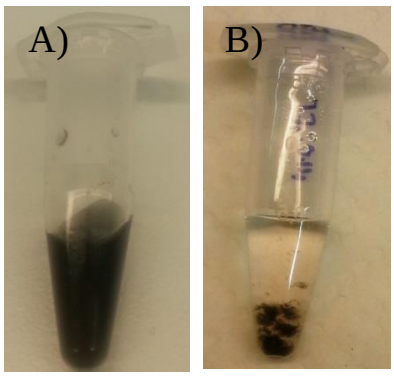

Figure 36 Comparison of sonicated (a) Poly$(G)_{20}$/SWCNT/YO-PRO-1 in H_2O and (b) ssDNA/SWCNT in H_2O.

To examine the fluorescence properties of the resulting ssDNA/SWCNT/YO-PRO-1 nanohybrids prepared with one-step mixing, the sample was titrated into H_2O. The fluorescence intensity of trimolecular nanostructure is higher than the same concentration of YO-PRO-1 solution (Figure 37-A). Moreover the nanohybrids were heated from 25^oC to 90^oC at the rate of 1^oC/min followed by a cooling cycle from 90^oC to 25^oC at the same rate (Figure 37-B). The cooling cycle (red spectrum) did not duplicate the heating cycle (black) and the fluorescence intensity at the end of the cycle was lower than the initial intensity illustrating that the same nanohybrid was not able to self-assemble again, instead different fluorescent structures have formed. These two analysis proved that in the trimolecular structure Poly$(G)_{20}$, SWCNT and YO-PRO-1 have noncovalent interactions. Thus this method is another technique to label CNTs with asymmetrical cyanine dyes.

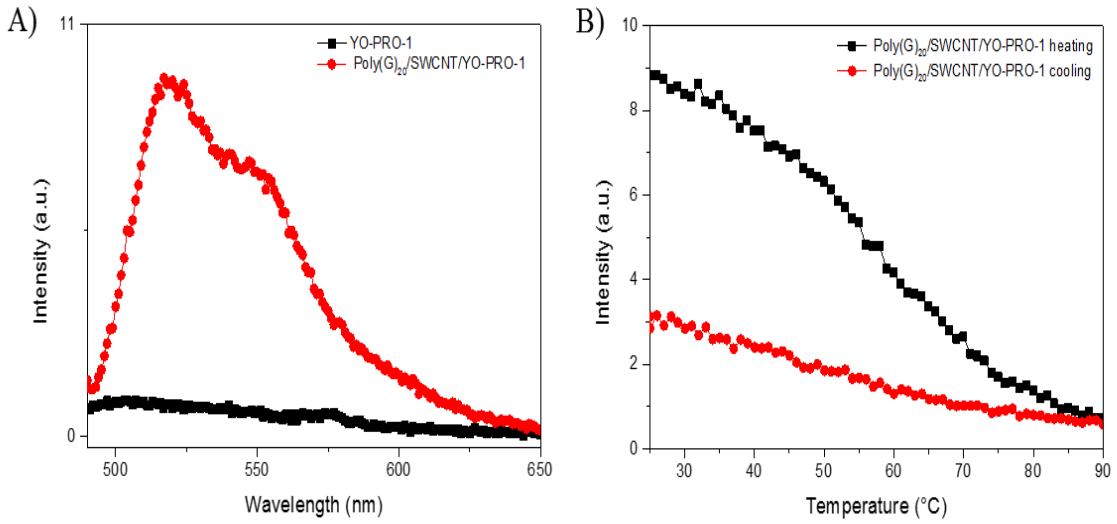

Figure 37 (A) The fluorescence spectra of Poly(G)$_{20}$/SWCNT/YO-PRO-1 trimolecular structure. (B) The fluorescence based thermal analysis of Poly(G)$_{20}$/SWCNT/YO-PRO-1 trimolecular structure

3.4.1 Confocal Microscopy

Confocal microscope was utilized to indicate whether these fluorescent nanohybrids can be visualized with fluorescent microscopy. Samples of trimolecular structure of ssDNA/SWCNT/dye hybrid were prepared on a glass slide and imaged with laser scanning confocal microscope. Excitation with a 488 nm laser results in an image demonstrating strongly fluorescent structures (Figure 38). These images demonstrate CNTs were labeled with asymmetrical cyanine dyes.

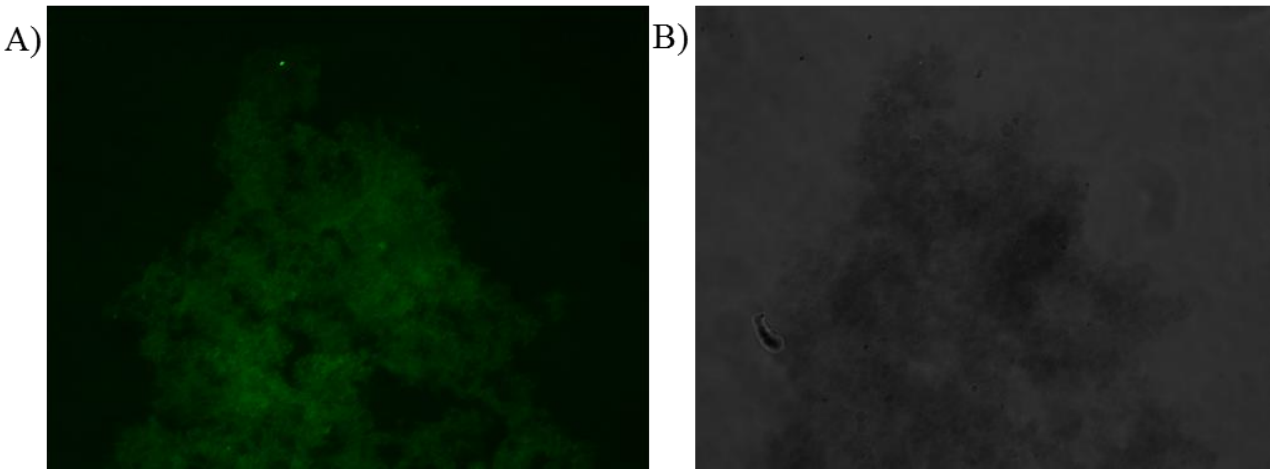

Figure 38 Confocal laser scanning microscopy images of ssDNA/SWCNT YOYO-1 system (A) fluorescence image, (B) the DIC image of the same spot.

3.4.2 Scanning Electron Microscopy (SEM)

Scanning electron microscopy was used to determine whether CNTs were dispersed separately or not. Figure 39 indicates that CNTs were individually dispersed. As a result of poor resolution of SEM, imaging of ssDNA and asymmetrical cyanine dyes over CNT was not possible. On the other hand, the interactions between ssDNA, CNT and asymmetrical cyanine dye molecules and the individually dispersed CNTs were visualized.

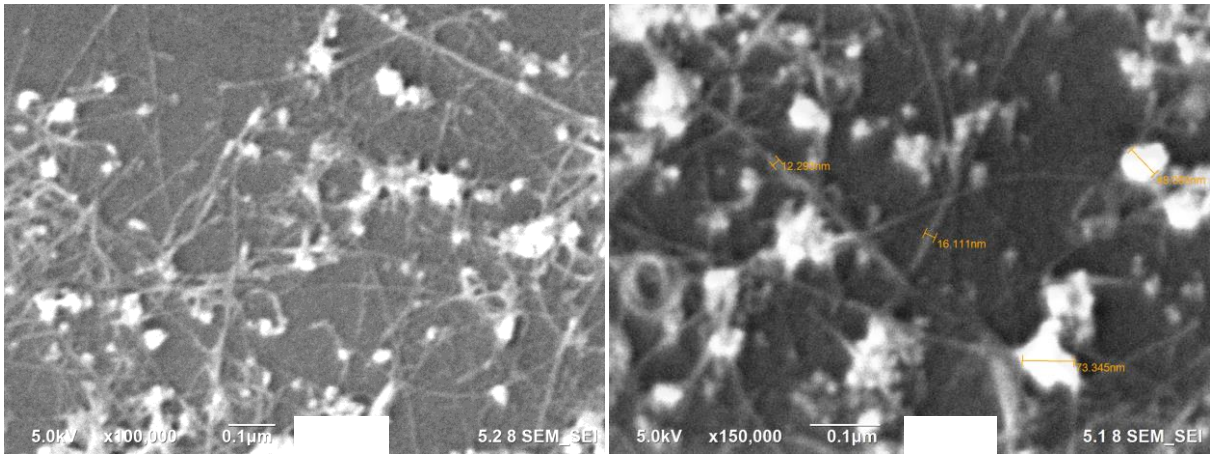

Figure 39 SEM images of ssDNA/CNT nanohybrids

3.4.3 Transmission Electron Microscopy (TEM)

Transmission electron microscopy was utilized to imaging ssDNA/CNT nanohybrids. The visualization of ssDNA/CNT nanohybrids was challenging. Owing to using 0.1 M NaCl solution for preparing ssDNA/CNT nanohybrids, dried salt particles blocked the visualizing of nanohybrids. Individually dispersed CNTs and salt contamination are shown in the Figure 40. TEM results were parallel as SEM results. Individually dispersed CNTs were presented once more.

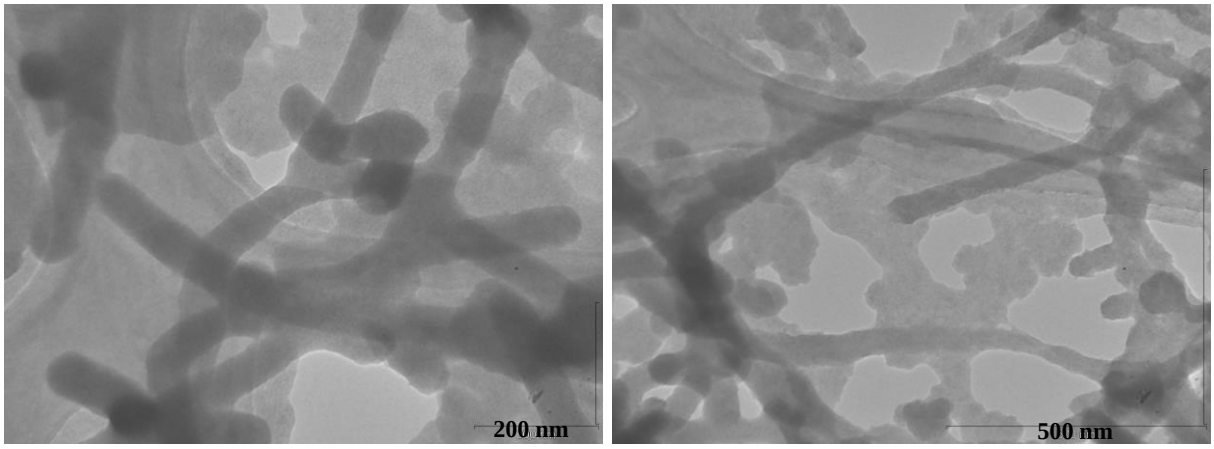

Figure 40 TEM images of ssDNA/CNT nanohybrids.

3.5 Binding of double stranded DNA (dsDNA) onto dye/CNT Template

Another method was developed for fluorescently labeling CNTs with asymmetrical cyanine dyes. In this method, YO-PRO-1/SWCNT nanohybrid was prepared as it was described in Chapter-1 and incubated with 0.08 μM dsDNA. We expected one of the two different scenarios to happen: (Figure 41).

1) The binding affinity of asymmetrical cyanine dye is higher for dsDNA than for CNTs. Thus, the binding between asymmetrical cyanine dyes and CNTs would rupture and dye molecules would interact with dsDNA.

2) Dye/CNT nanohybrid could have noncovalent interactions with dsDNA and could result in a trimolecular structure.

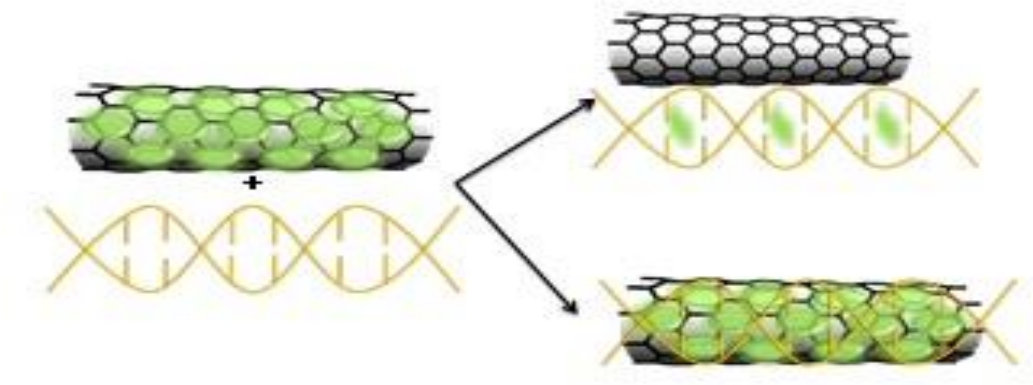

Figure 41 Schematic for two possible results of interactions between dsDNA and dye/CNT nanohybrids.

Figure 42 shows the fluorescence spectrum of YO-PRO-1/MWCNT (black) in comparison to the spectrum of the same nanohybrid incubated with dsDNA (red). As it is seen in the Figure 42 YO-PRO-1/MWCNT only shows background fluorescence. Its fluorescence was increased by addition of dsDNA.

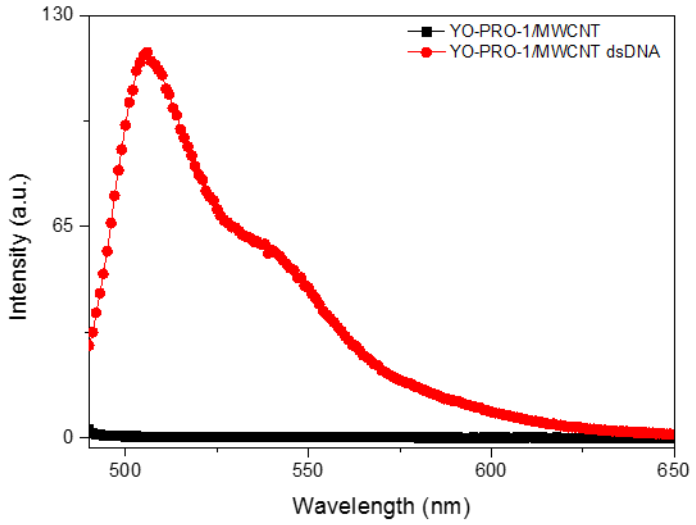

Figure 42 The fluorescence spectra of YO-PRO-1/MWCNT dsDNA system

To understand which of the scenarios caused the increase in fluorescence, the sample was heated from 25ºC to 90ºC at the rate of 1ºC/min followed by a cooling cycle from 90ºC to 25ºC at the same rate. In the Figure 43-A during heating process the fluorescence of the system was stable until around 50ºC. After 50ºC, the intensity started to decrease. Possible reason of this decrease on intensity is that the noncovalent interactions between the dye and the template is broken. Fluorescence intensity started to increase with the cooling cycle as demonstrated with the red spectrum. The cooling cycle did not duplicate the heating cycle and the fluorescence intensity at the end of the cycle was higher than the initial intensity illustrating that the same nanohybrid was not able to self-assemble again, instead different fluorescent structures have formed. Figure 43-B shows the control experiment. Same concentrations of YO-PRO-1/dsDNA were heated under same conditions. As it is seen in the Figure control system was resulted different than the fluorescent system. Our assumption is that after the incubation of dye/CNT dsDNA, trimolecular structure was obtained. This method also can be used for fluorescently labeling CNTs.

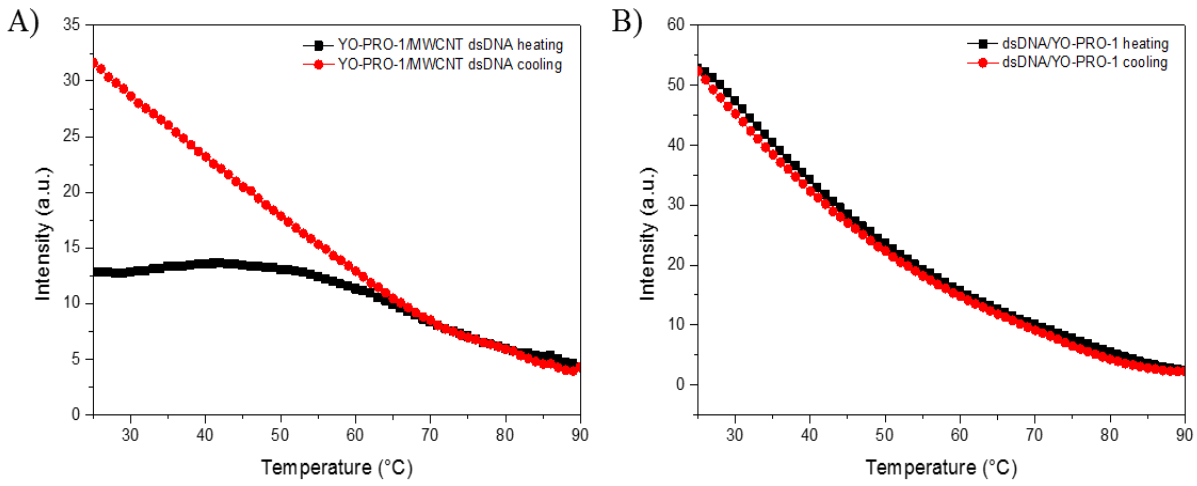

Figure 43 The fluorescence based thermal analysis of (A) YO-PRO-1/MWCNT dsDNA system. (B) YO-PRP-1/dsDNA system

4 Conclusion

In this chapter, noncovalent interactions between ssDNA, CNT and asymmetrical cyanine dyes were studied. First, ssDNA/CNT nanohybrids were prepared. The interactions between

ssDNA and CNT were analyzed with Raman Spectroscopy and TEM. The upshift at G' band at Raman spectrum proved the noncovalent interaction between ssDNA and CNT. Moreover, individually dispersed ssDNA/CNT nanohybrids were presented with TEM images. Second, non-fluorescent ssDNA/CNT nanohybrids were titrated with asymmetrical cyanine dyes and they became fluorescent. Moreover, one step trimolecular structure was prepared and observed fluorescence intensity once again. Last method was preparing dye/CNT dsDNA nanostructures. In this method dye/CNT nanostructures were incubated with dsDNA and they became fluorescent. Non-fluorescent dye/CNT nanostructure became fluorescent after incubation. Thermal analysis indicated dye/CNT nanostructures and dsDNA can form fluorescent trimolecular structures. As a result, a unique and feasible method for fluorescently labeling of CNTs was demonstrated.

CHAPTER 4 CONCLUSION

In conclusion, a novel and feasible method for the preparation of light absorbing and emitting CNTs was demonstrated. As a result of noncovalent interactions between asymmetrical cyanine dyes and CNTs, a light absorbing nano array was constructed. These nanoarrays can be tuned in terms of the absorbance wavelength by using dye molecules of different spectral properties.

When ssDNA wrapped CNTs interacted with asymmetrical cyanine dye molecules not only the absorbance intensity was altered but also the fluorescence intensity was increased several fold. That means ssDNA/CNT template delivered optimum binding sites for asymmetrical cyanine dyes to light up and create fluorescent nanostructures.

Our work demonstrates the first example that a fluorophore lights up when it binds CNTs, thus provides a novel approach for the fluorescent labeling of CNTs. We believe that these CNT/dye nanohybrids have large potential as photoactive materials. They can be potentially applied as photothermal materials that can convert the applied light irradiation into heat.

REFERENCES

1. Avouris, P., *Carbon nanotube electronics.* Chemical Physics, 2002. **281**(2–3): p. 429-445.
2. Baughman, R.H., A.A. Zakhidov, and W.A. de Heer, *Carbon Nanotubes--the Route Toward Applications.* Science, 2002. **297**(5582): p. 787-792.
3. Bonard, J.-M., et al., *Field emission from carbon nanotubes: the first five years.* Solid-State Electronics, 2001. **45**(6): p. 893-914.
4. M. Daenen, R.D.d.F., B. Hamers, P.G.A. Janssen, K. Schouteden, and M.A.J. Veld, *Wondrous World of Carbon Nanotubes. A Review of Current Carbon Nanotube Technologies*. 2003: Eindhoven Univeristy of Technology. p. p.93.
5. Ma, P.-C., et al., *Dispersion and functionalization of carbon nanotubes for polymer-based nanocomposites: A review.* Composites Part A: Applied Science and Manufacturing, 2010. **41**(10): p. 1345-1367.
6. Odom, T.W., J.-L. Huang, and C.M. Lieber, *Single-Walled Carbon Nanotubes.* Annals of the New York Academy of Sciences, 2002. **960**(1): p. 203-215.
7. Sahoo, N.G., et al., *Polymer nanocomposites based on functionalized carbon nanotubes.* Progress in Polymer Science, 2010. **35**(7): p. 837-867.
8. Meyyappan, M., *Carbon Nanotubes Science and Applications.* 2005.
9. Gogotsi, Y., *Nanotubes and Nanofibers* 2006.
10. Sharma, V.K., F. Jelen, and L. Trnkova, *Functionalized Solid Electrodes for Electrochemical Biosensing of Purine Nucleobases and Their Analogues: A Review.* Sensors (Basel, Switzerland), 2015. **15**(1): p. 1564-1600.
11. Yakobson, B.I. and P. Avouris, *Mechanical properties of carbon nanotubes.* Carbon Nanotubes, 2001. **80**: p. 287-327.
12. Hamon, M.A., et al., *Effect of Rehybridization on the Electronic Structure of Single-Walled Carbon Nanotubes.* Journal of the American Chemical Society, 2001. **123**(45): p. 11292-11293.
13. Yan, L., et al., *Low-toxic and safe nanomaterials by surface-chemical design, carbon nanotubes, fullerenes, metallofullerenes, and graphenes.* Nanoscale, 2011. **3**(2): p. 362-382.
14. Eatemadi, A., et al., *Carbon nanotubes: properties, synthesis, purification, and medical applications.* Nanoscale Research Letters, 2014. **9**.
15. Hou, P.-X., C. Liu, and H.-M. Cheng, *Purification of carbon nanotubes.* Carbon, 2008. **46**(15): p. 2003-2025.
16. Balasubramanian, K. and M. Burghard, *Chemically functionalized carbon nanotubes.* Small, 2005. **1**(2): p. 180-192.
17. Hirsch, A., *Functionalization of single-walled carbon nanotubes.* Angewandte Chemie-International Edition, 2002. **41**(11): p. 1853-1859.
18. Hirsch, A. and O. Vostrowsky, *Functionalization of carbon nanotubes.* Functional Molecular Nanostructures, 2005. **245**: p. 193-237.
19. Tasis, D., et al., *Chemistry of carbon nanotubes.* Chemical Reviews, 2006. **106**(3): p. 1105-1136.
20. Wu, H.C., et al., *Chemistry of carbon nanotubes in biomedical applications.* Journal of Materials Chemistry, 2010. **20**(6): p. 1036-1052.
21. Coleman, J.N., U. Khan, and Y.K. Gun'ko, *Mechanical reinforcement of polymers using carbon nanotubes.* Advanced Materials, 2006. **18**(6): p. 689-706.

22. Zheng, M., et al., *DNA-assisted dispersion and separation of carbon nanotubes.* Nature Materials, 2003. **2**(5): p. 338-342.
23. Zheng, M., et al., *Structure-based carbon nanotube sorting by sequence-dependent DNA assembly.* Science, 2003. **302**(5650): p. 1545-1548.
24. Bhattacharyya, S., E. Kymakis, and G.A.J. Amaratunga, *Photovoltaic Properties of Dye Functionalized Single-Wall Carbon Nanotube/Conjugated Polymer Devices.* Chemistry of Materials, 2004. **16**(23): p. 4819-4823.
25. Meng, L., C. Fu, and Q. Lu, *Advanced technology for functionalization of carbon nanotubes.* Progress in Natural Science, 2009. **19**(7): p. 801-810.
26. Heister, E., et al., *Are carbon nanotubes a natural solution? Applications in biology and medicine.* ACS Appl Mater Interfaces, 2013. **5**(6): p. 1870-91.
27. He, H., et al., *Carbon Nanotubes: Applications in Pharmacy and Medicine.* BioMed Research International, 2013. **2013**: p. 12.
28. Nakayama-Ratchford, N., et al., *Noncovalent Functionalization of Carbon Nanotubes by Fluorescein−Polyethylene Glycol: Supramolecular Conjugates with pH-Dependent Absorbance and Fluorescence.* Journal of the American Chemical Society, 2007. **129**(9): p. 2448-2449.
29. Yoshimura, S.H., et al., *Fluorescence Labeling of Carbon Nanotubes and Visualization of a Nanotube−Protein Hybrid under Fluorescence Microscope.* Biomacromolecules, 2011. **12**(4): p. 1200-1204.
30. Meng, L.J., C.L. Fu, and Q.H. Lu, *Advanced technology for functionalization of carbon nanotubes.* Progress in Natural Science, 2009. **19**(7): p. 801-810.
31. Prakash, R., et al., *Visualization of individual carbon nanotubes with fluorescence microscopy using conventional fluorophores.* Applied Physics Letters, 2003. **83**(6): p. 1219.
32. Zhang, J., et al., *Photoluminescence and Electronic Interaction of Anthracene Derivatives Adsorbed on Sidewalls of Single-Walled Carbon Nanotubes.* Nano Letters, 2003. **3**(3): p. 403-407.
33. Martin, R.B., et al., *Functionalized Carbon Nanotubes with Tethered Pyrenes: Synthesis and Photophysical Properties.* The Journal of Physical Chemistry B, 2004. **108**(31): p. 11447-11453.
34. Satake, A., Y. Miyajima, and Y. Kobuke, *Porphyrin - Carbon nanotube composites formed by noncovalent polymer wrapping.* Chemistry of Materials, 2005. **17**(4): p. 716-724.
35. Casey, J.P., S.M. Bachilo, and R.B. Weisman, *Efficient photosensitized energy transfer and near-IR fluorescence from porphyrin-SWNT complexes.* Journal of Materials Chemistry, 2008. **18**(13): p. 1510-1516.
36. Rahman, G.M.A., et al., *Electronically interacting single wall carbon nanotube-porphyrin nanohybrids.* Journal of Materials Chemistry, 2006. **16**(1): p. 62-65.
37. Pan, B., et al., *Effects of Carbon Nanotubes on Photoluminescence Properties of Quantum Dots.* The Journal of Physical Chemistry C, 2008. **112**(4): p. 939-944.
38. Didenko, V.V., et al., *Visualization of Individual Single-Walled Carbon Nanotubes by Fluorescent Polymer Wrapping.* Nano Letters, 2005. **5**(8): p. 1563-1567.
39. Otobe, K., et al., *Fluorescence visualization of carbon nanotubes by modification with silicon-based polymer.* Nano Letters, 2002. **2**(10): p. 1157-1160.

40. Yuan, W.Z., et al., *Wrapping carbon nanotubes in pyrene-containing poly(phenylacetylene) chains: Solubility, stability, light emission, and surface photovoltaic properties.* Macromolecules, 2006. **39**(23): p. 8011-8020.
41. Fernandez-Suarez, M. and A.Y. Ting, *Fluorescent probes for super-resolution imaging in living cells.* Nat Rev Mol Cell Biol, 2008. **9**(12): p. 929-943.
42. Armitage, B.A., *Cyanine Dye-DNA Interactions: Intercalation, Groove Binding, and Aggregation.* 2005.
43. Nygren, J., N. Svanvik, and M. Kubista, *The interactions between the fluorescent dye thiazole orange and DNA.* Biopolymers, 1998. **46**(1): p. 39-51.
44. Rye, H.S., et al., *Stable Fluorescent Complexes of Double-Stranded DNA with Bis-Intercalating Asymmetric Cyanine Dyes - Properties and Applications.* Nucleic Acids Research, 1992. **20**(11): p. 2803-2812.
45. Carlsson, C., et al., *Optical and Photophysical Properties of the Oxazole Yellow DNA Probes YO and YOYO.* The Journal of Physical Chemistry, 1994. **98**(40): p. 10313-10321.
46. Chiu, C.F., N. Dementev, and E. Borguet, *Fluorescence Quenching of Dyes Covalently Attached to Single-Walled Carbon Nanotubes.* Journal of Physical Chemistry A, 2011. **115**(34): p. 9579-9584.
47. Zhu, Z., et al., *Single-walled carbon nanotube as an effective quencher.* Analytical and Bioanalytical Chemistry, 2010. **396**(1): p. 73-83.
48. R. Saito, G.D.a.M.S.D., *Physical Properties of Carbon Nanotubes*. Imperial College Press, London. 1998.
49. Frolov, A.I., et al., *Molecular mechanisms of salt effects on carbon nanotube dispersions in an organic solvent (N-methyl-2-pyrrolidone).* Chemical Science, 2012. **3**(2): p. 541-548.
50. Baskaran, D., J.W. Mays, and M.S. Bratcher, *Noncovalent and Nonspecific Molecular Interactions of Polymers with Multiwalled Carbon Nanotubes.* Chemistry of Materials, 2005. **17**(13): p. 3389-3397.
51. Mandal, A. and A.K. Nandi, *Noncovalent Functionalization of Multiwalled Carbon Nanotube by a Polythiophene-Based Compatibilizer: Reinforcement and Conductivity Improvement in Poly(vinylidene fluoride) Films.* Journal of Physical Chemistry C, 2012. **116**(16): p. 9360-9371.
52. Fürstenberg, A. and E. Vauthey, *Ultrafast Excited-State Dynamics of Oxazole Yellow DNA Intercalators.* The Journal of Physical Chemistry B, 2007. **111**(43): p. 12610-12620.
53. Albertorio, F., et al., *Base dependent DNA-carbon nanotube interactions: activation enthalpies and assembly-disassembly control.* Nanotechnology, 2009. **20**(39): p. 395101.
54. Wang, Y., *Theoretical Evidence for the Stronger Ability of Thymine to Disperse SWCNT than Cytosine and Adenine: self-stacking of DNA bases vs their cross-stacking with SWCNT.* The journal of physical chemistry. C, Nanomaterials and interfaces, 2008. **112**(37): p. 14297-14305.